THE RELATION OF LOW TEMPERATURE DEFORMATION AND SUSCEPTIBILITY TO HYDROGEN EMBRITTLEMENT OF AUSTENITIC STAINLESS STEELS

Peter Francis Scardigno

NAVAL POSTGRADUATE SCHOOL
Monterey, California

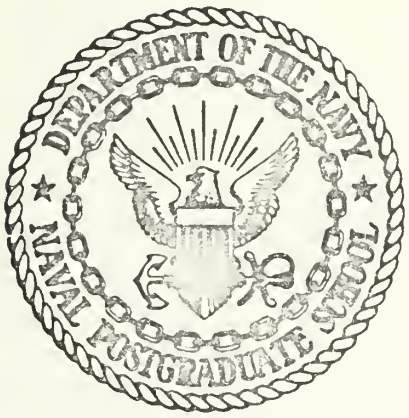

THESIS

THE RELATION OF LOW TEMPERATURE DEFORMATION AND SUSCEPTIBILITY TO HYDROGEN EMBRITTLEMENT OF AUSTENITIC STAINLESS STEELS

by

Peter Francis Scardigno

December 1974

Thesis Advisor: A. J. Perkins

SECURITY CLASSIFICATION OF THIS PAGE (When Data Entered)

REPORT DOCUMENTATION PAGE

READ INSTRUCTIONS BEFORE COMPLETING FORM

1. REPORT NUMBER	2. GOVT ACCESSION NO. / 3. RECIPIENT'S CATALOG NUMBER
4. TITLE (and Subtitle): The Relation of Low Temperature Deformation and Susceptibility to Hydrogen Embrittlement of Austenitic Stainless Steels	5. TYPE OF REPORT & PERIOD COVERED: Master's Thesis; December 1974
	6. PERFORMING ORG. REPORT NUMBER
7. AUTHOR(s): Peter Francis Scardigno	8. CONTRACT OR GRANT NUMBER(s)
9. PERFORMING ORGANIZATION NAME AND ADDRESS: Naval Postgraduate School, Monterey, California 93940	10. PROGRAM ELEMENT, PROJECT, TASK AREA & WORK UNIT NUMBERS
11. CONTROLLING OFFICE NAME AND ADDRESS: Naval Postgraduate School, Monterey, California 93940	12. REPORT DATE: December 1974
	13. NUMBER OF PAGES: 114
14. MONITORING AGENCY NAME & ADDRESS (if different from Controlling Office): Naval Postgraduate School, Monterey, California 93940	15. SECURITY CLASS. (of this report): Unclassified
	15a. DECLASSIFICATION/DOWNGRADING SCHEDULE

16. DISTRIBUTION STATEMENT (of this Report)

Approved for public release; distribution unlimited.

17. DISTRIBUTION STATEMENT (of the abstract entered in Block 20, if different from Report)

18. SUPPLEMENTARY NOTES

19. KEY WORDS (Continue on reverse side if necessary and identify by block number)

Low Temperature Deformation
Hydrogen Embrittlement
Austenitic Stainless Steels

20. ABSTRACT (Continue on reverse side if necessary and identify by block number)

An investigation into the relation of low temperature deformation and susceptibility to hydrogen embrittlement of two austenitic stainless steels was conducted. Two candidate materials for cryogenic service, commercial stainless steels 304-L, and 21-6-9, were utilized for the experiments. These materials were subjected to deformation at various strain rates and temperatures in an attempt to induce

DD FORM 1 JAN 73 1473 (Page 1)

EDITION OF 1 NOV 65 IS OBSOLETE
S/N 0102-014-6601

SECURITY CLASSIFICATION OF THIS PAGE (When Data Entered)

Block 20 - ABSTRACT (Cont.)

partial and/or complete martensitic transformation. Tensile strength, yield strength, percent tensile elongation, percent reduction in area, notched tensile strength, percent notched tensile elongation, percent reduction in area (notched), and notched/unnotched strength ratios were tabulated as baseline data.

The two alloys were then subjected to interrupted tensile tests at various temperatures in which samples were exposed to a cathodic hydrogen charging procedure at various values of tensile pre-strain. The mechanical parameters mentioned above were tabulated and compared graphically. Fractographic and metallographic analysis of fractured specimens were performed. The combined effect of hydrogen embrittlement and phase transformation is discussed.

The Relation of Low Temperature Deformation and Susceptibility to Hydrogen Embrittlement of Austenitic Stainless Steels

by

Peter Francis Scardigno
Lieutenant Commander, United States Navy
B.S., United States Naval Academy, 1965

Submitted in partial fulfillment of the
requirements for the degree of

MASTER OF SCIENCE IN MECHANICAL ENGINEERING

ABSTRACT

An investigation into the relation of low temperature deformation and susceptibility to hydrogen embrittlement of two austenitic stainless steels was conducted. Two candidate materials for cryogenic service, commercial stainless steels 304-L, and 21-6-9, were utilized for the experiments. These materials were subjected to deformation at various strain rates and temperatures in an attempt to induce partial and/or complete martensitic transformation. Tensile strength, yield strength, percent tensile elongation, percent reduction in area, notched tensile strength, percent notched tensile elongation, percent reduction in area (notched), and notched/unnotched strength ratios were tabulated as baseline data.

The two alloys were then subjected to interrupted tensile tests at various temperatures in which samples were exposed to a cathodic hydrogen charging procedure at various values of tensile pre-strain. The mechanical parameters mentioned above were tabulated and compared graphically. Fractographic and metallographic analysis of fractured specimens were performed. The combined effect of hydrogen embrittlement and phase transformation is discussed.

TABLE OF CONTENTS

LIST OF TABLES

LIST OF ILLUSTRATIONS

FIGURE

FIGURE

FIGURE

FIGURE

FIGURE

ACKNOWLEDGEMENT

The author wishes to express his appreciation for the guidance and encouragement given by Dr. A. J. Perkins and Dr. G. R. Edwards in pursuit of this investigation. He wishes to acknowledge Mr. R. Edwards of the Material Science section of the Mechanical Engineering department for his patient assistance and advice for this project and to thank the Machine Facility for the construction of the required equipment and specimens. Last, but not least, he wishes to thank his wife, Diane, for patiently following this investigation to its completion.

I. INTRODUCTION

The advent of the energy crises has summoned with it a plethora of ideas which could alleviate its impact in the immediate future. Recent alternatives to fossil fuels which are being proposed include, the more efficient utilization of fission by broader use of breeder reactors, controllable fusion processes, harnessing tidal and wind power, and more reliance on geothermal and solar energy among others. In a recent paper Dr. Derek P. Gregory proposed a new alternative not hither-to mentioned, the so-called "hydrogen economy" [1]. He believes that the increasing reliance on electrical energy which is generated mainly by fossil fuels will, in the near future, result in an electric economy. Although presently this may seem advantageous, the depletion of fossil fuels will have a detrimental effect on this trend. The ultimate replacement of fossil fuels probably will be the direct conversion of nuclear energy into electricity, but there will be many areas where this will not be either efficient or reliable. Many segments of the economy, both public and private, rely heavily on direct fossil fuel conversion. With its inevitable depletion an alternate source such as hydrogen must be used. Hydrogen can easily be made adaptable to many of the present energy conversion systems. Its abundance from the synthesis of sea water makes it an almost unlimited fuel. The method by which the synthesis of hydrogen occurs will become a moot question with the

increasing proliferation of nuclear power plants along our sea coasts.

Proposals for hydrogen powered vehicles and airplanes have increasingly become vogue among many academic circles. However, one of the most realistic and immediately obtainable proposals for the use of hydrogen is that of its replacement for natural gas. Little modification would be needed for its adaptation to the natural gas distribution system. Environmental studies have praised the usage of hydrogen as an energy source, but the one area which has not been discussed is its effect on the system which will be used to store, transport and handle it. Hydrogen is primarily found in two states -- liquid and gaseous depending on its use. The area of research where little work has been done is on the type storage and carriage materials that will be used in conjunction with hydrogen. In almost all popular literature promoting hydrogen, little attention is given to the need for appropriate storage and carriage materials. This may be a serious omission of attention, as hydrogen is well known to have very deleterious effects on certain types of metals. These effects can be referred to by the general term "hydrogen embrittlement." It is this potential embrittlement problem which is the focus of this study.

Two austenitic stainless steels were chosen as candidate cryogenic materials in this study. These are 304-L and Armco 21-6-9 (NITRONIC-40). Table I lists the metallurgical properties of each of these metals. Their excellent

characteristics at low temperatures [2],[3] and reported resistance to hydrogen embrittlement made them the prime candidates in this investigation.

II. MARTENSITIC TRANSFORMATIONS

Historically, the behavior of martensitic transformation has been questioned as early as 1370 A.D. by Osesme. Until the Bain model [4] was proposed in 1924, men only took advantage of the obvious strengthening characteristics with little understanding of any of the associated effects. Since then, numerous areas of steel processing have evolved based on martensitic transformations.

In this particular study 304-L and 21-6-9 stainless steel are exposed to martensitic transformation mechanisms. Both these steels are crystallographically structured as FCC when in the stable austenitic phase, which generally encompasses the ambient to above ambient temperature range. The transformation sequence of 304-L is $\gamma \rightarrow \varepsilon \rightarrow \alpha$ phase change which is characteristic of the morphological change of austenite to martensite in a metastable austenitic stainless steel [5]. It is reported that 21-6-9 does not undergo any martensitic transformation [6]. The relative stability of the FCC γ structure of 304-L and 21-6-9 are primarily the result of combining the following elements: nickel, manganese, carbon, nitrogen along with cromium and molybdenum. Hopefully this combination will result in a relatively stable austenitic structure with a wide temperature span.

Epsilon (ε) martensite is the second, and in some cases the last, phase in the morphogical chain of the martensitic transformation process in 304-L. It is characterized by a

HCP crystal structure which appears as small plates about 1μ wide. Mangonon and Thomas [5] have conducted extensive tests on 304-L which verified the existence of ε phase in the transitional chain to martensite. Structurally, ε martensite is a perfect HCP structure which exhibits no ferromagnetic properties. The nucleation of ε martensite is generally the result of a strain-induced transformation from the austenitic phase which can be assisted thermally. It can either be formed independently of α martensite or co-exist with it.

Alpha (α) martensite is a BCC crystallographic structure and is the final phase in the transitional chain to martensite of 304-L. Its formation only occurs as a result of plastic deformation and subsequent to formation of ε martensite. Nucleation of α martensite occurs heterogeneously at intersections of ε bands either where ε bands abut twins or the grain boundaries. Its appearance will first be of a needle-like structure and subsequently grow to become lathe-like [5]. α martensite may coexist with ε martensite but its amount will grow at the expense of a decrease in ε martensite. It will, however, not be found to exist independently of ε martensite. Because it is ferromagnetic in nature, permability studies such as one proposed by Maxwell [7] can be used to determine the amount of α present in a metal. By utilizing this characteristic, calibration curves can be constructed which when compared optically can be used to determine the amount of martensite that forms within a relatively short time span.

The term strain-induced martensite [8], used in the preceding explanations of the morphogical chain of martensitic transformation, indicates that the martensite formed is a direct result of plastic deformation. It is characterized by a fine particle or lath type structure which can occur in elongated clusters delineating the slip bands with strained martensite.

III. HYDROGEN EMBRITTLEMENT

The influence of hydrogen on metals has been the object of a great deal of study for at least two decades. It was not until recently that the term hydrogen embrittlement was classified into various types. The three basic classifications of these embrittlement phenomena are: (1) hydrogen-reaction embrittlement, (2) hydrogen-environmental embrittlement and (3) internal-hydrogen embrittlement [16].

Hydrogen-reaction embrittlement occurs when hydrogen combines with one of the constituents in a metal to form a hydride [9] or some other embrittlement phase. This combination may either occur in the molecular or disassociated form of hydrogen. In carbon based steels, hydrogen has a propensity to react with the carbon constitutent to form methane gas in various internal imperfections of the metal. This formation results in extremely high internal pressures which assist in crack propagations. In addition, the combination of carbon and hydrogen results in a decarbonization process which will further reduce the strength of a metal. Hydrogen reaction embrittlement is considered a non-reversible process.

Hydrogen-environmental embrittlement occurs primarily when a metal is continually exposed to a hydrogen environment. Exposure to an elevated temperature and pressure enhances this type of embrittlement. The adsorption and dissociation of hydrogen molecules in or on the microscopic

surface cracks generated by plastic deformations such as cyclical loading [9] result in the susceptible metal being less ductile, and displaying a faster crack growth rate than would occur in an inert environment. Once the hydrogen-environment is removed, the embrittlement mechanism no longer exists, hence this is considered to be a reversible process.

The most insidious type of embrittlement and one which can not be detected until a "fait accompli" situation arises is that of internal-hydrogen embrittlement. Hydrogen enters metal in the dissociated form and recombines with itself as hydrogen molecules. The exact embrittlement mechanism of these molecules to the stress gradients and imperfections present is still being debated [11][12], but the final result is known. There is generally a loss of ductility, subcritical crack growth, and an increase in strength [6]. Evidence presently available indicates that internal-hydrogen embrittlement occurs most rapidly at or near room temperature [6]. Metallurgical processes which include plating, cathodic charging, pickling, and welding [13][14] have all exhibited a high propensity toward internal-hydrogen susceptibility. The reversibility of this type of embrittlement is dependent upon two factors. One is its dependence upon exposure time since a diffusional process is involved when a metal is subjected to a hydrogen source. The second factor depends upon whether flaws, fissures or cracks have formed. If they have not formed and if the hydrogen source is removed no embrittlement will result.

Present studies have indicated that austenitic stainless steels and more specifically metals that retain an FCC crystallographic structure are less susceptible to hydrogen embrittlement than those that have undergone a martensitic transformation to a BCC structure [8][10]. Epsilon (ε) martensite, dislocation pileups and phase interfaces (α and ε martensites) provide paths of high diffusivity, thereby enhancing hydrogen diffusion. These are analogously referred to as short-circuit diffusion paths [15]. When this short circuit diffusion is coupled with hydrogen-dislocation interactions, embrittlement of the metal results.

IV. EXPERIMENTAL PROCEDURES

A. SPECIMEN COMPOSITION, PROCESSING, GEOMETRIES, TESTING APPARATUS

The two stainless steels used during this investigation are 304-L and 21-6-9. Table I lists their chemical compositions and previous preparations prior to their testing. Figure 1 lists the geometrical configuration used for the notched and unnotched specimens.

The annealed samples of 304-L and 21-6-9 were tested on an Instron machine (Fig. 2). Two crosshead rates were chosen to obtain a variation in strain rates so that a strain-induced martensitic transformation could occur. The strain rates utilized were .005 in/min and 1 in/min. The second parameter varied was temperature. The temperatures selected for this investigation were 300°K, 195°K and 76°K. The ambient temperature of the laboratory was 300°K. The use of methyl alcohol coupled with dry ice produced 195°K. The use of a liquid nitrogen bath produced 76°K. Since a wide temperature spectrum was required, an attachment to the Instron Machine was designed which allowed specimens to be immersed in the various cryogenic baths (Fig. 3). Reduced temperatures were used to promote stress-assisted martensitic transformations.

TABLE I. METALLURGICAL CONDITION OF TEST ALLOYS

Alloy	Form and Condition	Composition (%)	Specimen Geometries
304-L	SHEET, MILLED ANNEALED	.03C, 2Mn, 19Cr 10Ni, 1Si, .045P .030S	a, b
21-6-9 ARMCO NITRONIC-40	ROUND, ROLLED MILLED ANNEALED	.04C, 9Mn, 20.5Cr 6.5Ni, .3N	a, b

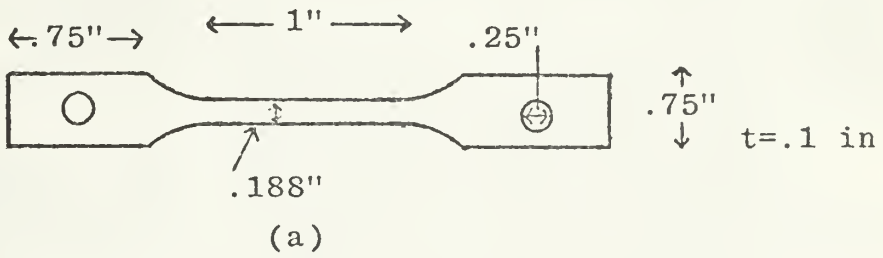

(a)

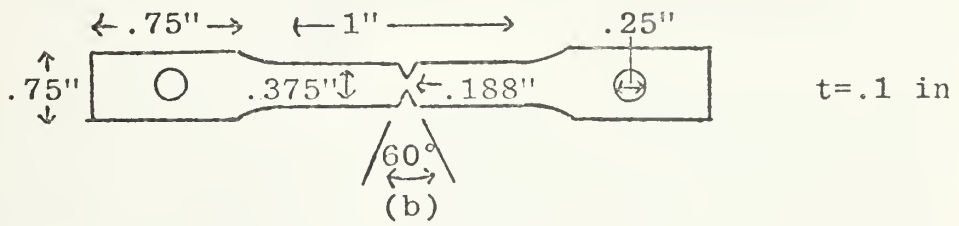

(b)

FIGURE 1. GEOMETRICAL CONFIGURATIONS OF NOTCHED AND UNNOTCHED SPECIMENS

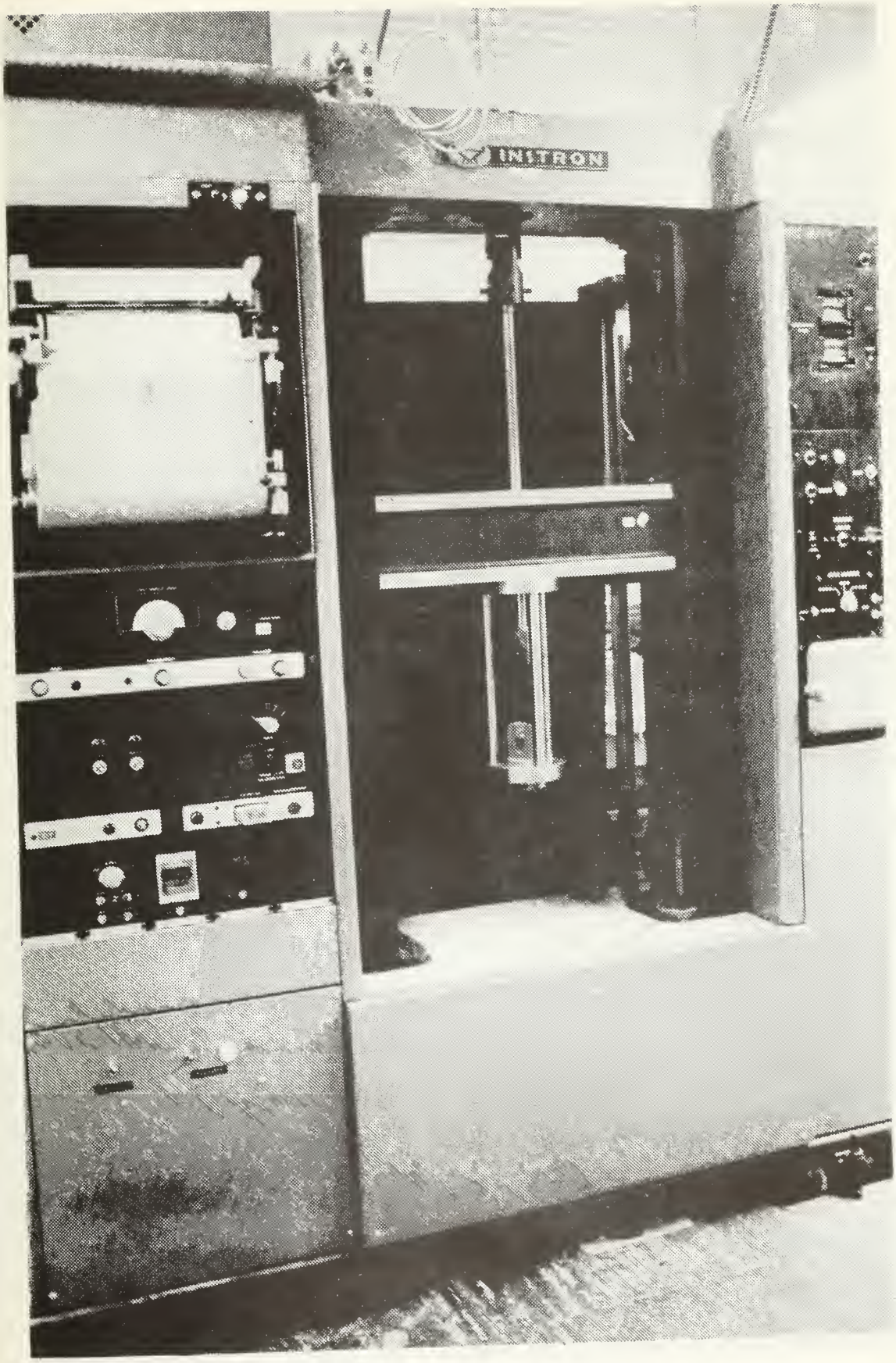

FIGURE 2. INSTRON TESTING MACHINE

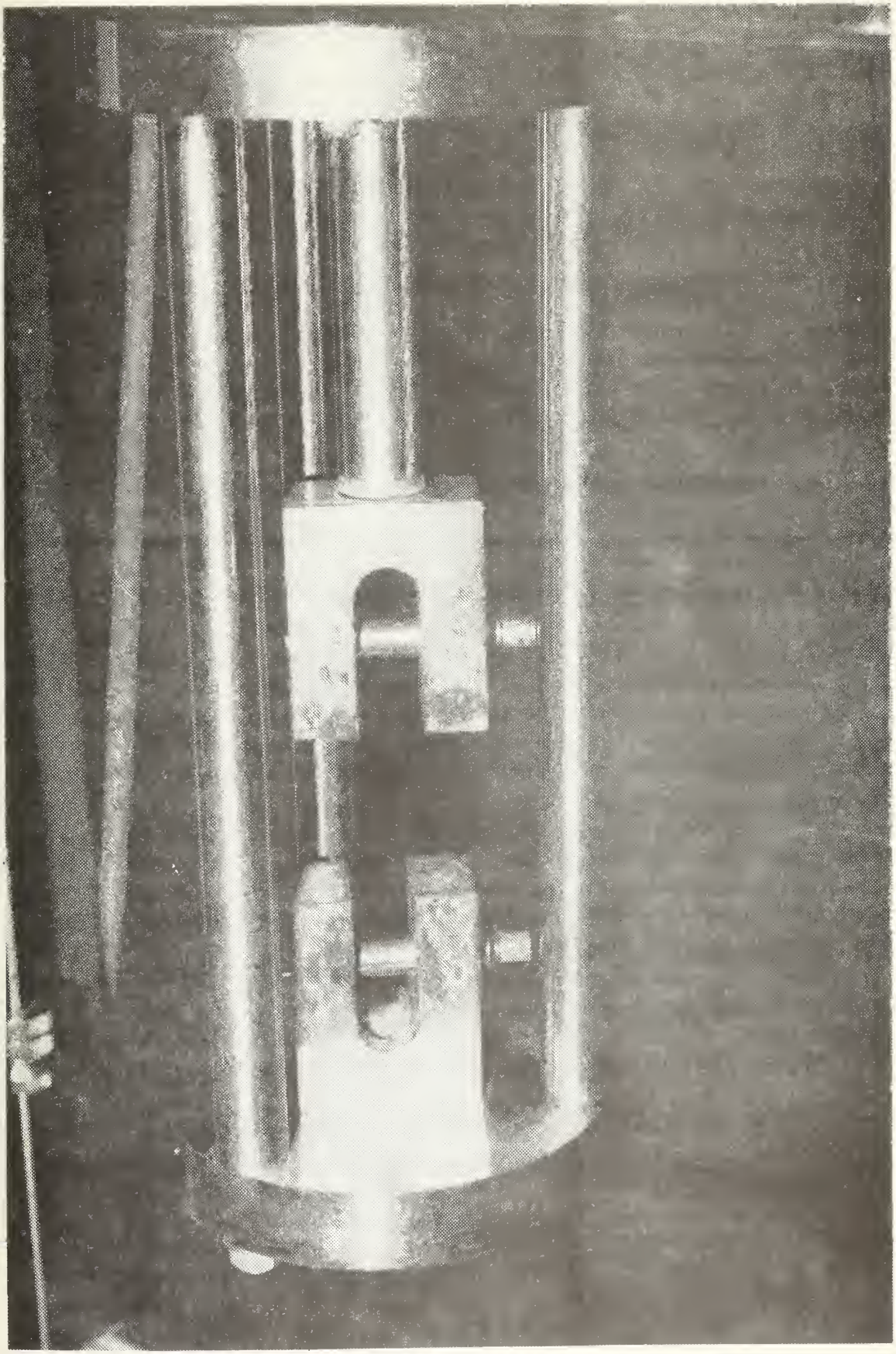

FIGURE 3. TESTING ATTACHMENT

B. BASELINE DATA COMPILATION

To provide baseline data, notched and unnotched specimens were strained at each temperature for each strain rate indicated. Values of tensile strength, yield strength, percent tensile elongation, percent reduction in area, notched tensile strength, percent notched tensile elongation, percent reduction in area (notched), and notched/unnotched strength ratios were tabulated. Because of the length of time required only one test per specimen per parameter was performed. Upon completion of this testing routine, values obtained which did not follow any predictable trend were retested and an average value was used in lieu of the original test data.

C. INTERRUPTED TESTING PROCEDURE

The major portion of the testing was dedicated to the testing of cathodically charged specimens. This charging procedure is explained in part D of this section. Unnotched samples were subjected to various percents of pre-strain before charging. These intervals were 0% pre-strain, 12%-31% pre-strain, and 32%-50% pre-strain for both 304-L and 21-6-9. Because the notched samples had much less total elongation, they were only pre-strained at two values. These were 0% pre-strain and 2%-15% pre-strain. As with the base data tests, these charged specimens were strained at the temperatures and crosshead rates previously indicated.

Upon completion of the charging procedure, the tensile tests were continued until failure occurred. Data recorded

was the same as with previous tests with the exception of one additional value. A measure of flow stress was measured upon the commencement of the interrupted tensile test. This value was used to determine the effect of the cathodic charging procedure as an embrittling mechanism on the specimens.

D. CATHODIC CHARGING PROCEDURE

The method of inducing internal-hydrogen embrittlement was by cathodically charging the specimens. Green and Latanision [16] discuss several variations of electrochemical techniques used in their investigations of the embrittlement phenomenon. Discussions with Dr. Green [17] indicated that the method which could be used consisted of specimens being immersed in a 4% (by weight) H_2SO_4 solution with five drops of cathodic poison [14] added per liter of solution. The cathodic poison consisted of two grams of Phosphorous dissolved in 40 ml of CS_2. Platinum was used as the anode while the specimen was used as the cathode. Figure 4 is the setup used during this study. A D.C. current of 1.5 amps at five volts was utilized to assist the absorption rate of hydrogen into the metal. The current density on the exposed part of the specimen was 79.78 amps/in^2 which was approximately the value recommended by Dr. Green for this particular study. The permeability, diffusivity, and solubility of hydrogen in austenitic stainless steels are governed by these relationships [18].

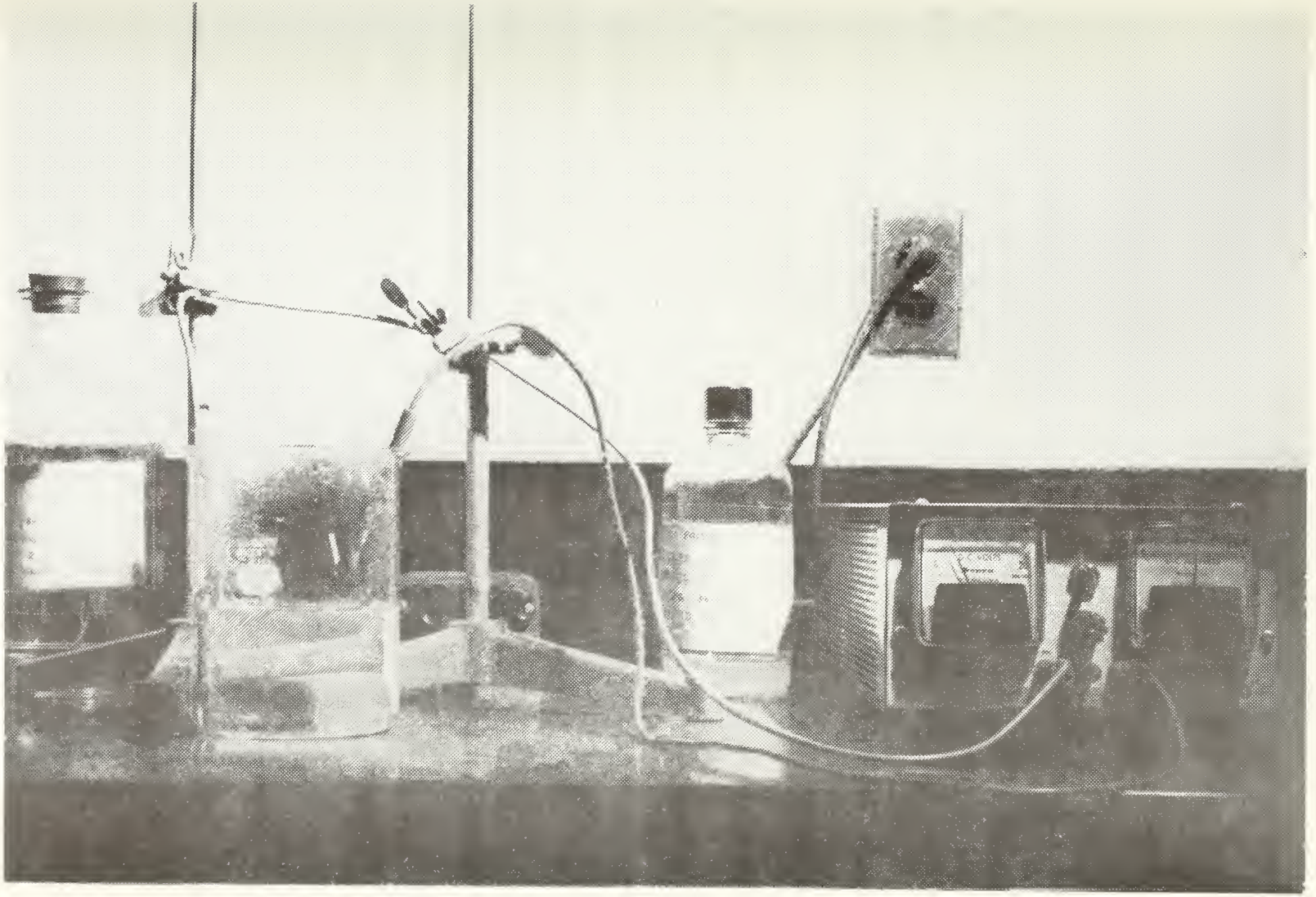

FIGURE 4. CATHODIC CHARGING APPARATUS

$$\phi = 6 \times 10^{-3} \exp\left(\frac{-14,300}{RT}\right) \frac{cc(NTP)}{(cm - atm^{\frac{1}{2}}S)} \quad (1)$$

$$D = 4.7 \times 10^{-3} \exp\left(\frac{-12,900}{RT}\right) \frac{cm^2}{S} \quad (2)$$

$$C = 1.28 \exp\left(\frac{-1400}{RT}\right) \frac{cc(NTP)}{(cm^3 - atm^{\frac{1}{2}})} \quad (3)$$

The normalized hydrogen concentration profile resulting from diffusion-controlled absorption into a semi-infinite solid exposed to hydrogen at constant fugacity is [15]

$$\frac{C}{C_0} = \text{erfc}\left(\frac{X}{2\sqrt{DT}}\right) \quad (4)$$

where C is the hydrogen concentration at X, C_0 is the surface concentration, D is the diffusivity and t is the exposure time. Since the specimens were charged for one-half hour on each side facing the platinum anode the normalized concentration value at the end of one hour in the center of the specimen would be 1. Therefore, saturation was achieved via this charging procedure and for this duration. Once austenitic and/or martensitic stainless steels become charged there is no perceptible loss of hydrogen for periods of at least three months at room temperatures [19]. Generally, the only manner in which hydrogen can rapidly diffuse from these metals is by being subjected to elevated temperatures for short intervals.

V. RESULTS AND DISCUSSION

A. GRAPHICAL RESULTS

The results of this portion of the investigation are plotted in the following thirteen graphs (Figs. 5 through 17). These consist of six basic stress vs. strain graphs and two summations of baseline data graphs of ultimate tensile strength, yield strength, percent tensile elongation, and toughness vs. temperature. The remaining six graphs plot the effect of cathodic charging on the specimens utilizing percent elongation prior to charging as an abscissa and values of normalized elongation, and increase in flow stress as the ordinate. Normalized elongation is defined as follows:

$$\frac{K - J}{H - J} \tag{5}$$

where H is the total elongation of an uncharged specimen at fracture, J the percent elongation prior to charging, and K the total elongation of the charged fractured specimen. Increase in flow stress is a measure of the increase in yield stress after specimens have been subjected to the charging procedure.

Since hydrogen embrittlement is a low strain rate phenomenon, and the data compiled for the notched and unnotched specimens at the high strain rate was inconclusive, no attempt was made to plot and compare their results. The sensitivity of the notched and the unnotched samples was mainly

related to the temperature effect and not the charging procedure.

The estimated experimental scatter was subject to the single-sample test analysis. The major sources of error were from the differences in the thermal expansion coefficients of the testing rig and from the specimens which were not geometrically identical in fabrication. Experimental scatter limits are indicated on each plot.

B. DISCUSSION OF GRAPHICAL RESULTS AND CORRELATION WITH FRACTOGRAPHIC RESULTS

The stress vs. strain plots clearly indicate that for the uncharged tests, 21-6-9 was capable of achieving higher strength levels at a given temperature and strain rate than that of 304-L. For the low strain rate, 21-6-9 was also more ductile than 304-L but for the fast strain rate 304-L was more ductile. This indicates that 21-6-9 is an inherently tougher material than 304-L, but the toughness differential becomes less at high strain rates and low temperatures. At 76°K, 304-L's toughness exceeds 21-6-9's for the low strain rate but is approximately equal for the high strain rate. This is because 304-L results to a martensitic structure at this temperature which manifests itself as high strength. Both metals exhibited generally higher strength and ductility values at lower temperatures and higher strain rates than were expected. Figures 11 and 12 summarize the effect of the temperature and strain rate on the measured parameters.

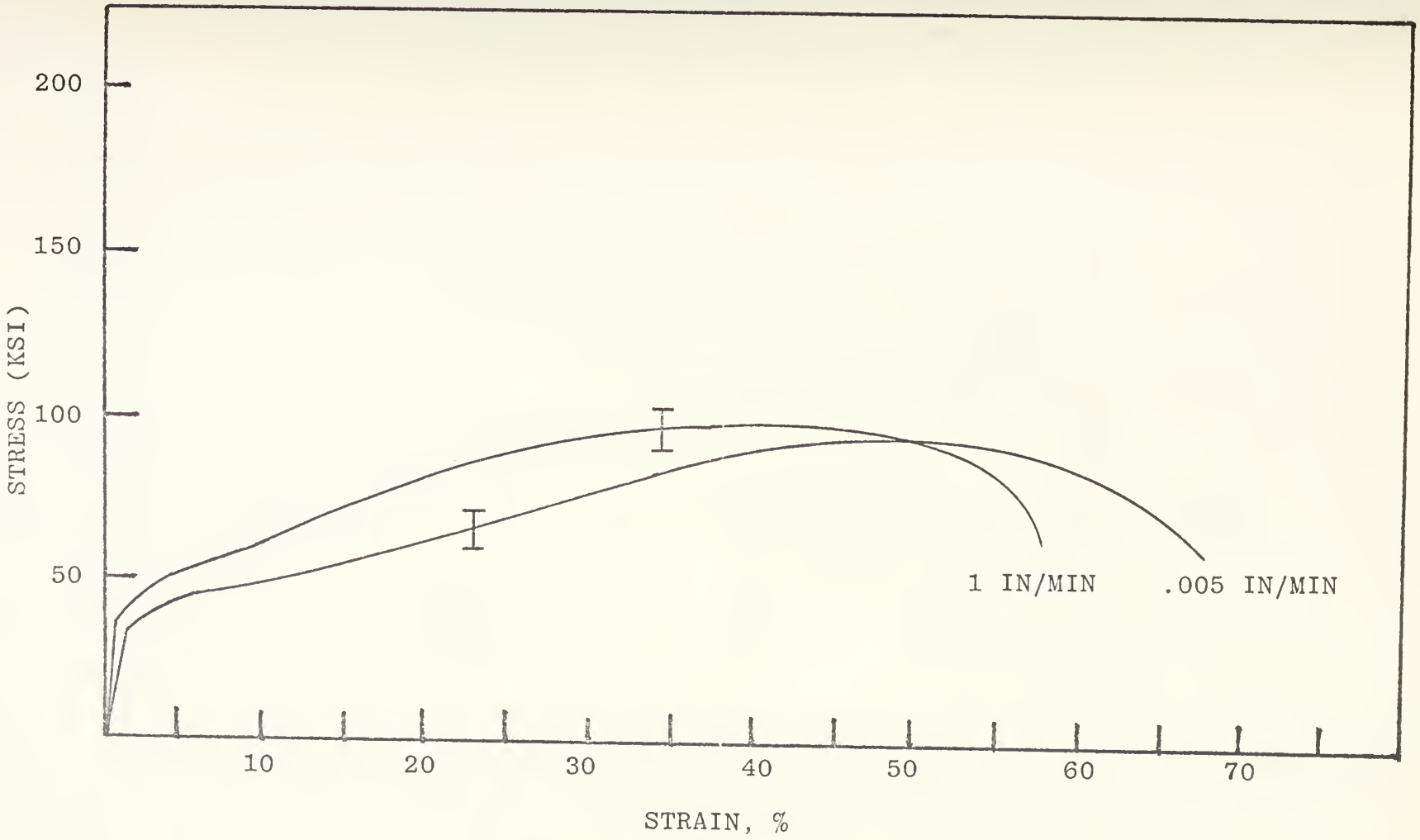

FIGURE 5. TRUE STRESS VS TRUE STRAIN, 304-L, 300°K

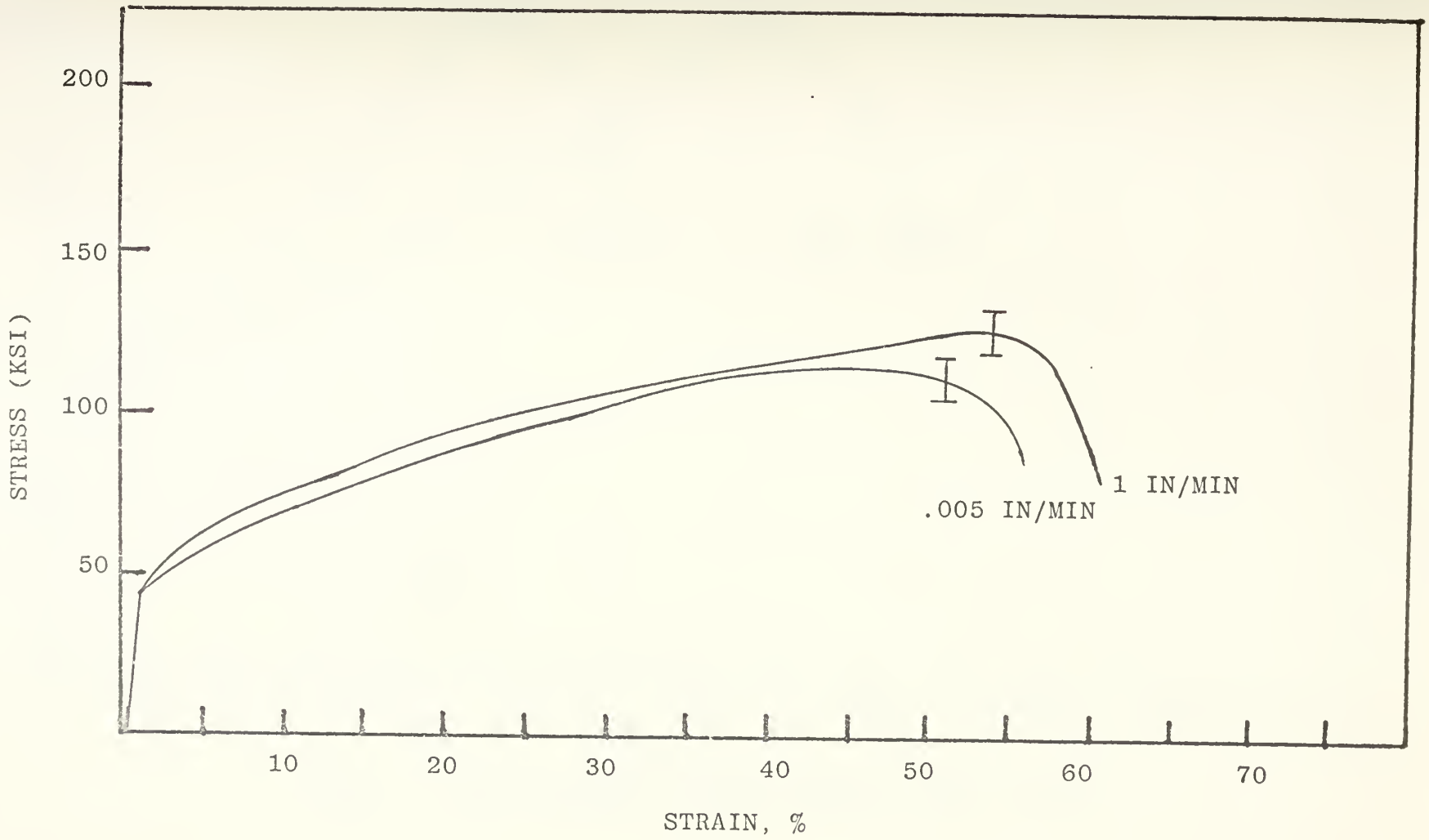

FIGURE 6. TRUE STRESS VS TRUE STRAIN, 304-L, 195°K

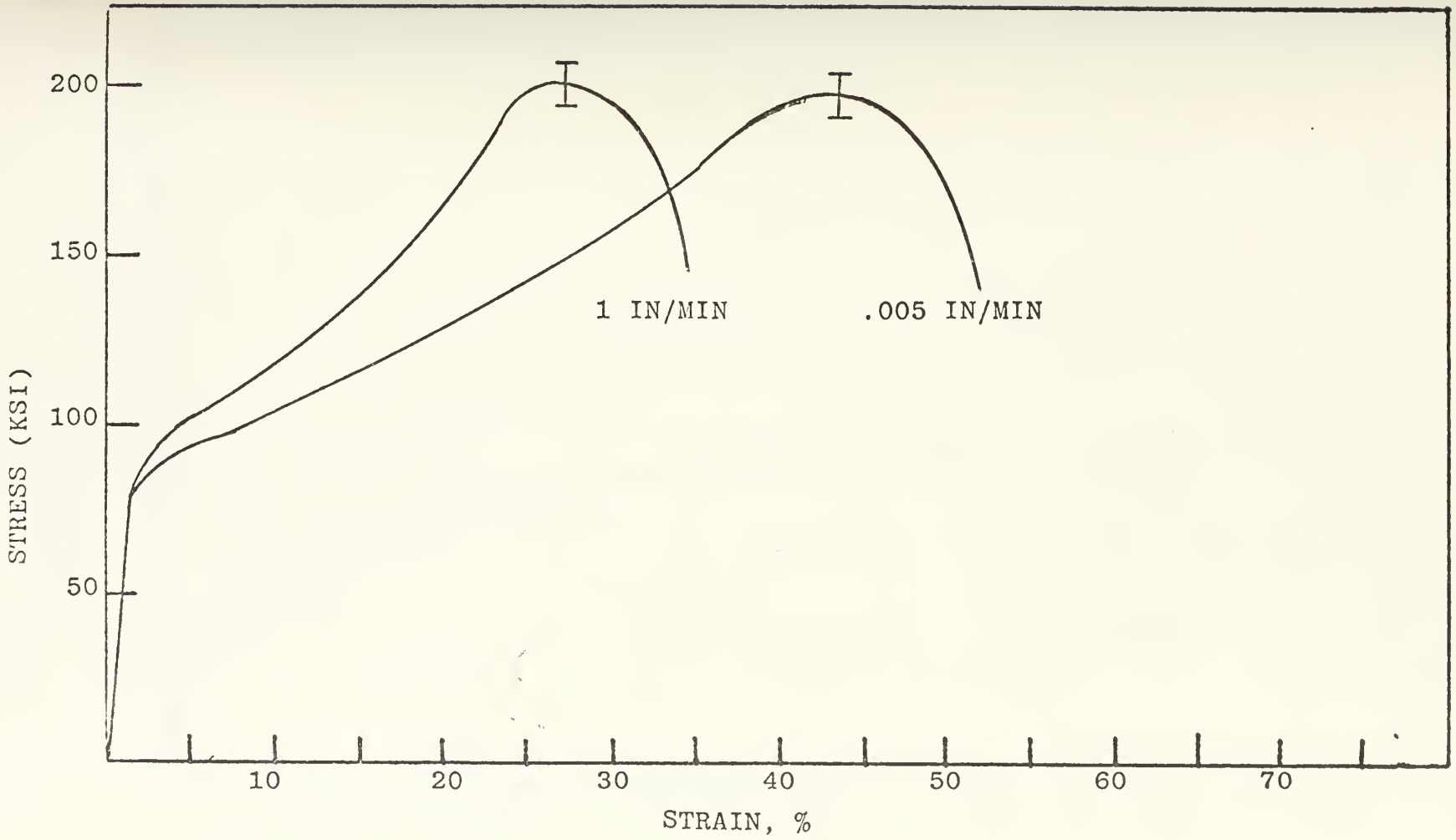

FIGURE 7. TRUE STRESS VS TRUE STRAIN, 304-L, 76°K

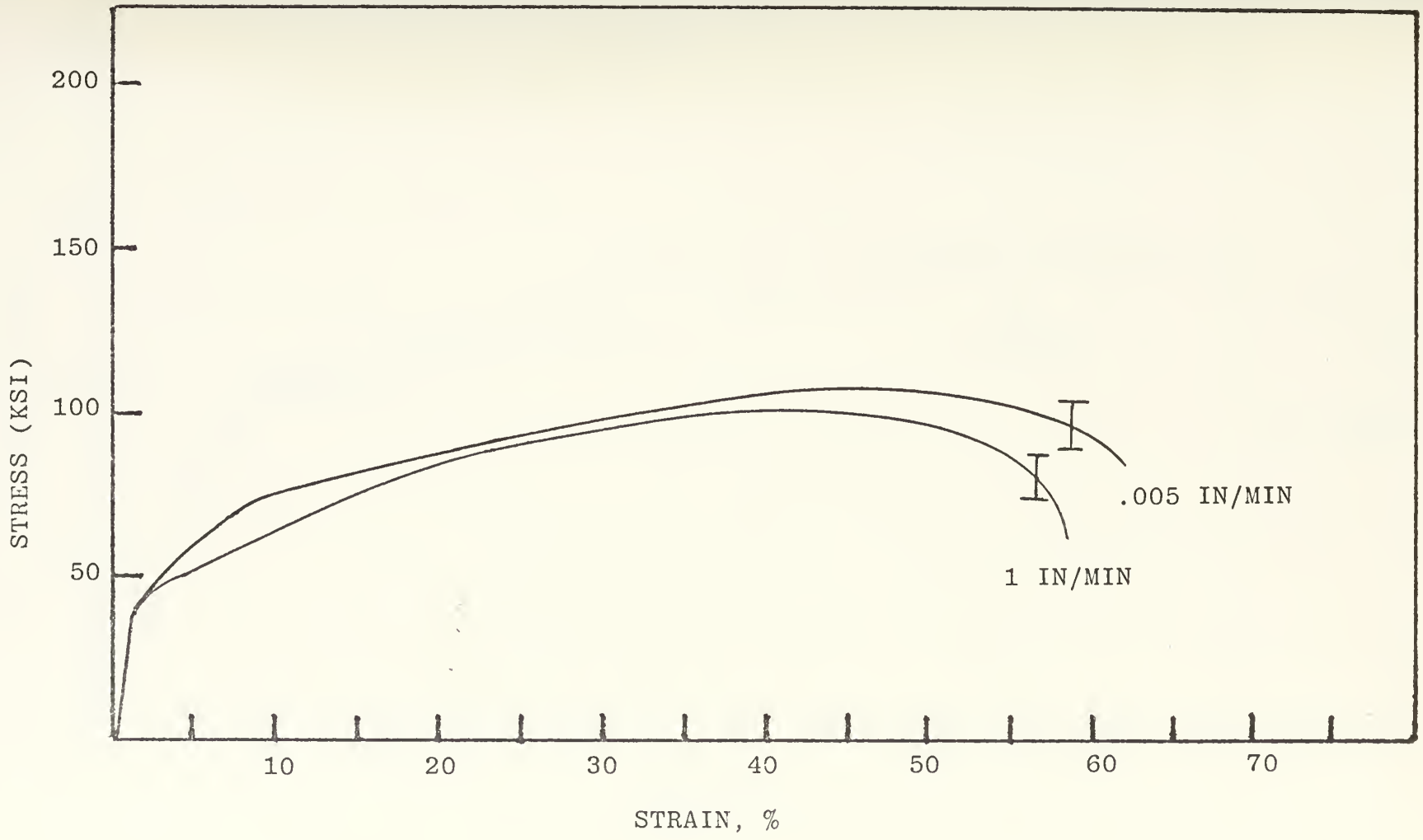

FIGURE 8. TRUE STRESS VS TRUE STRAIN, 21-6-9, 300°K

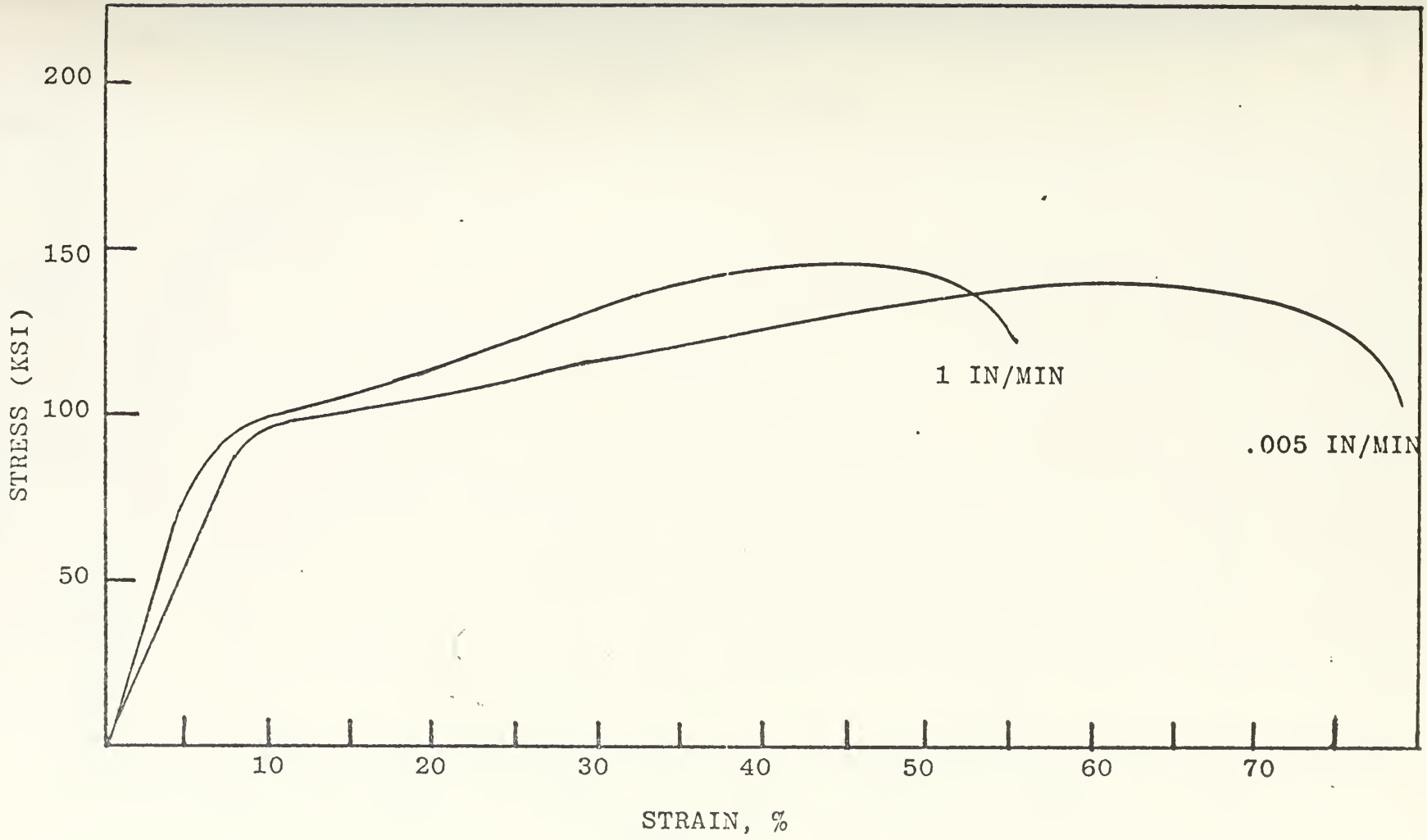

FIGURE 9. TRUE STRESS VS TRUE STRAIN, 21-6-9, 195°K

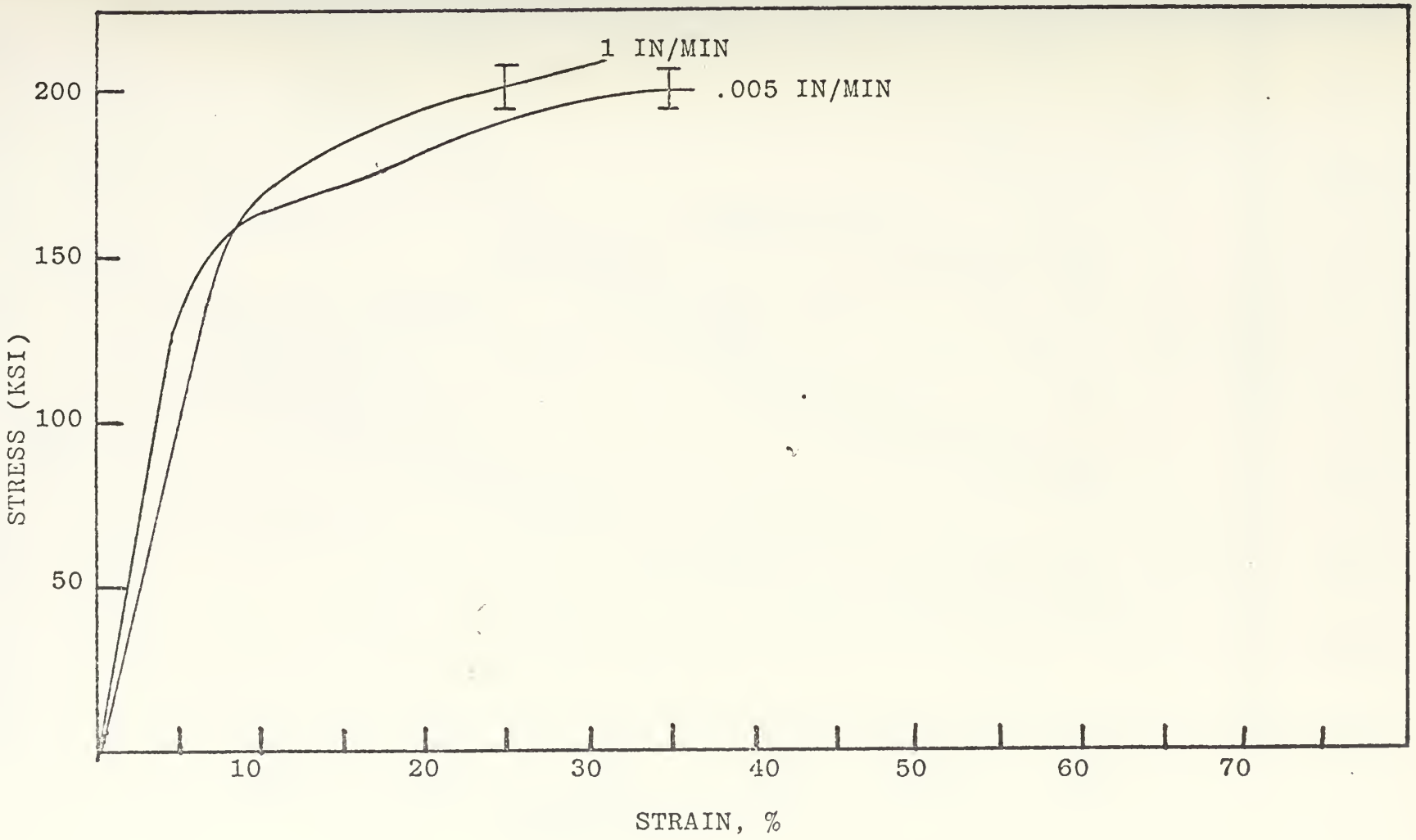

FIGURE 10. TRUE STRESS VS TRUE STRAIN, 21-6-9, 76°K

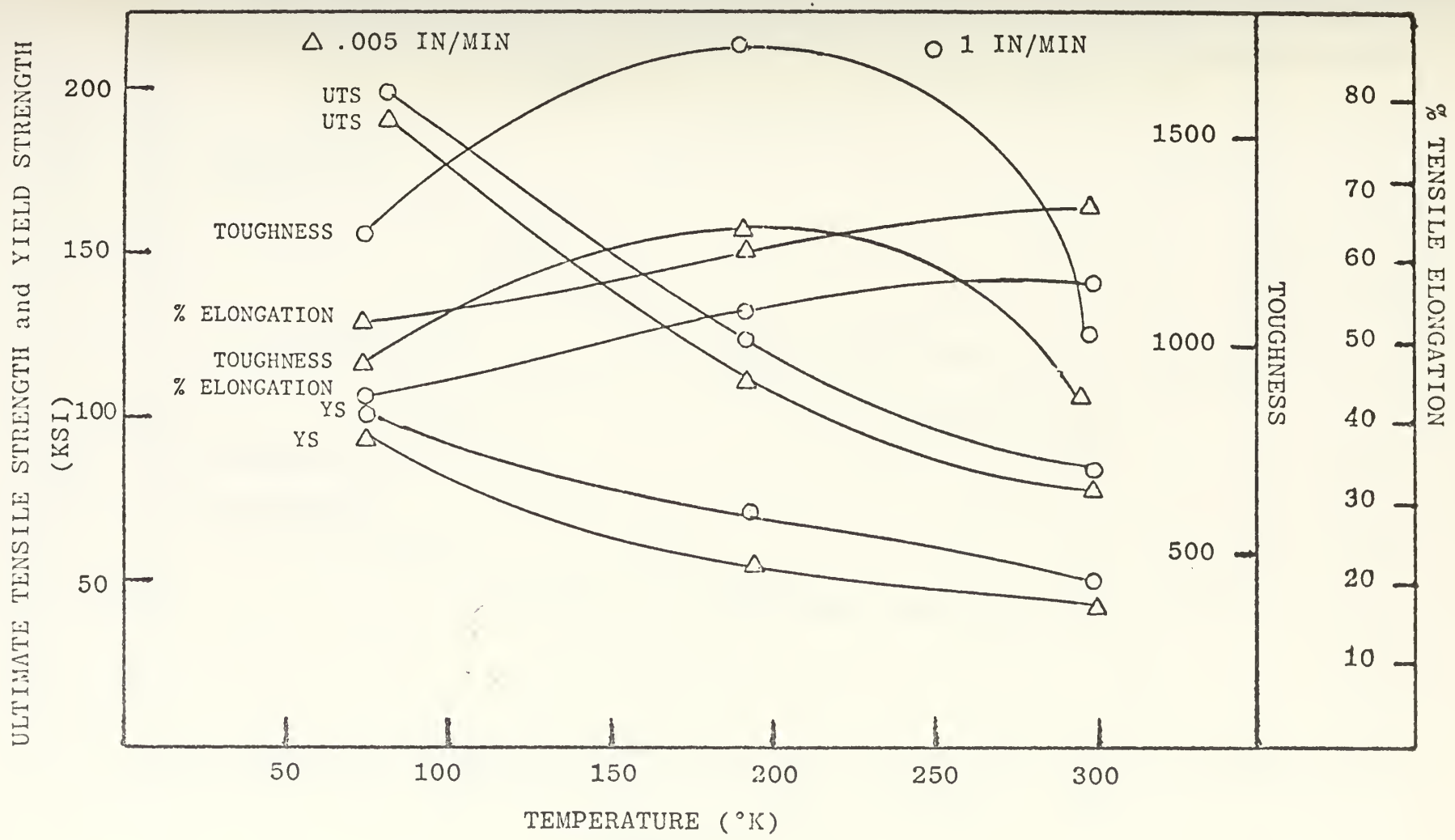

FIGURE 11. ULTIMATE TENSILE STRENGTH, YIELD STRENGTH, PERCENT TENSILE ELONGATION AND TOUGHNESS VS TEMPERATURE, 304-L

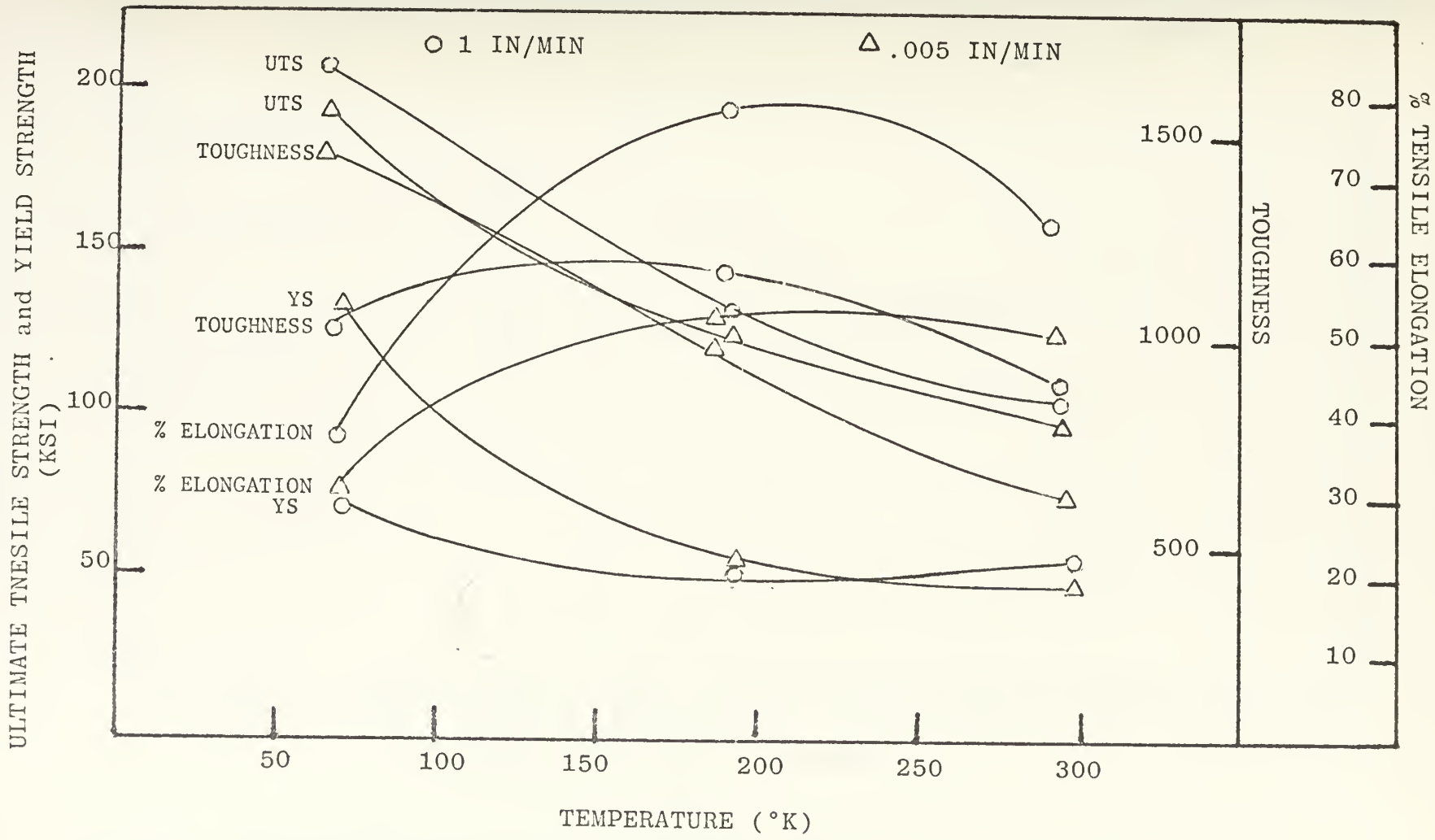

FIGURE 12. ULTIMATE TENSILE STRENGTH, YEILD STRENGTH, PERCENT TENSILE ELONGATION AND TOUGHNESS VS TEMPERATURE, 21-6-9

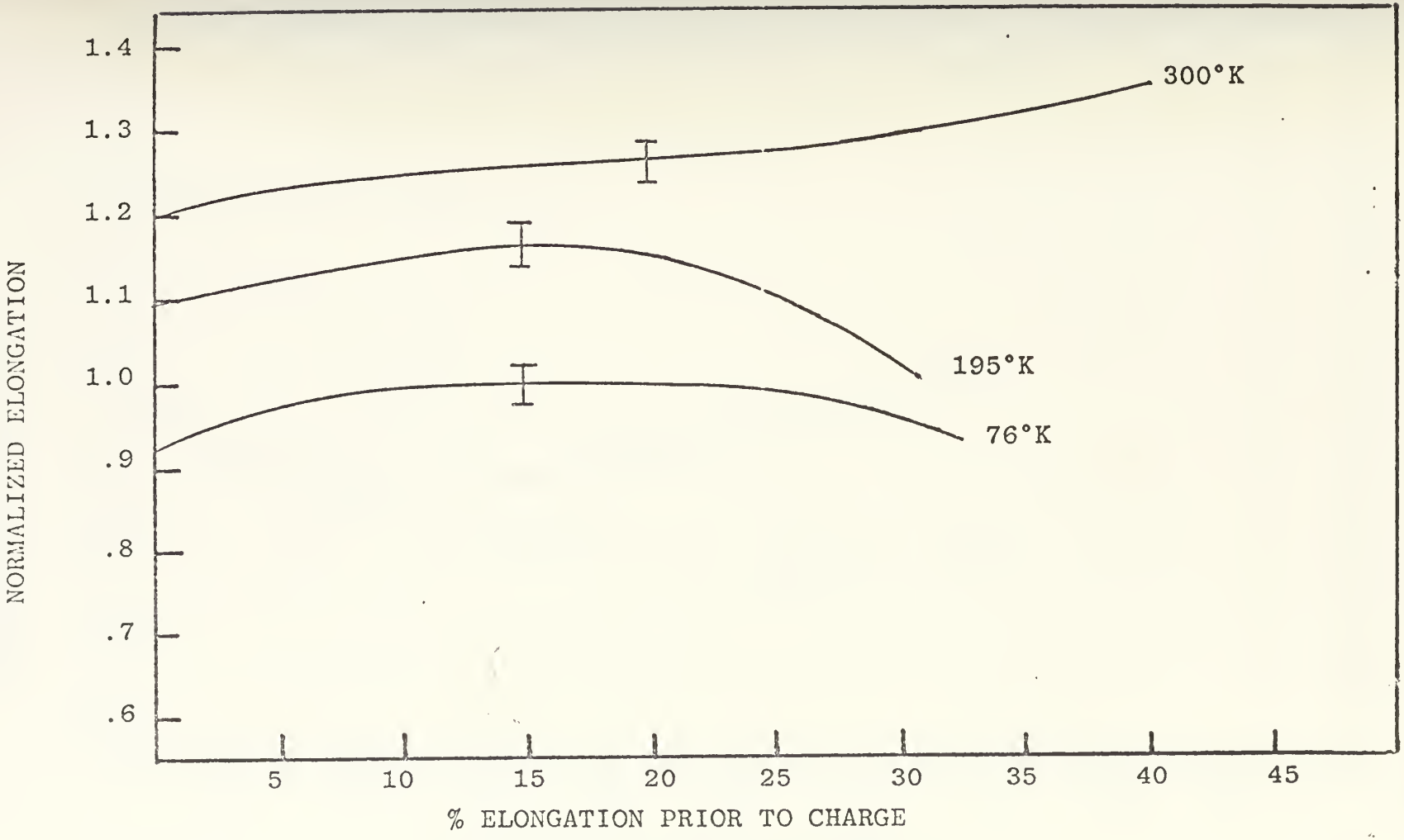

FIGURE 13. NORMALIZED ELONGATION VS PERCENT ELONGATION PRIOR TO CHARGE, UNNOTCHED, 304-L

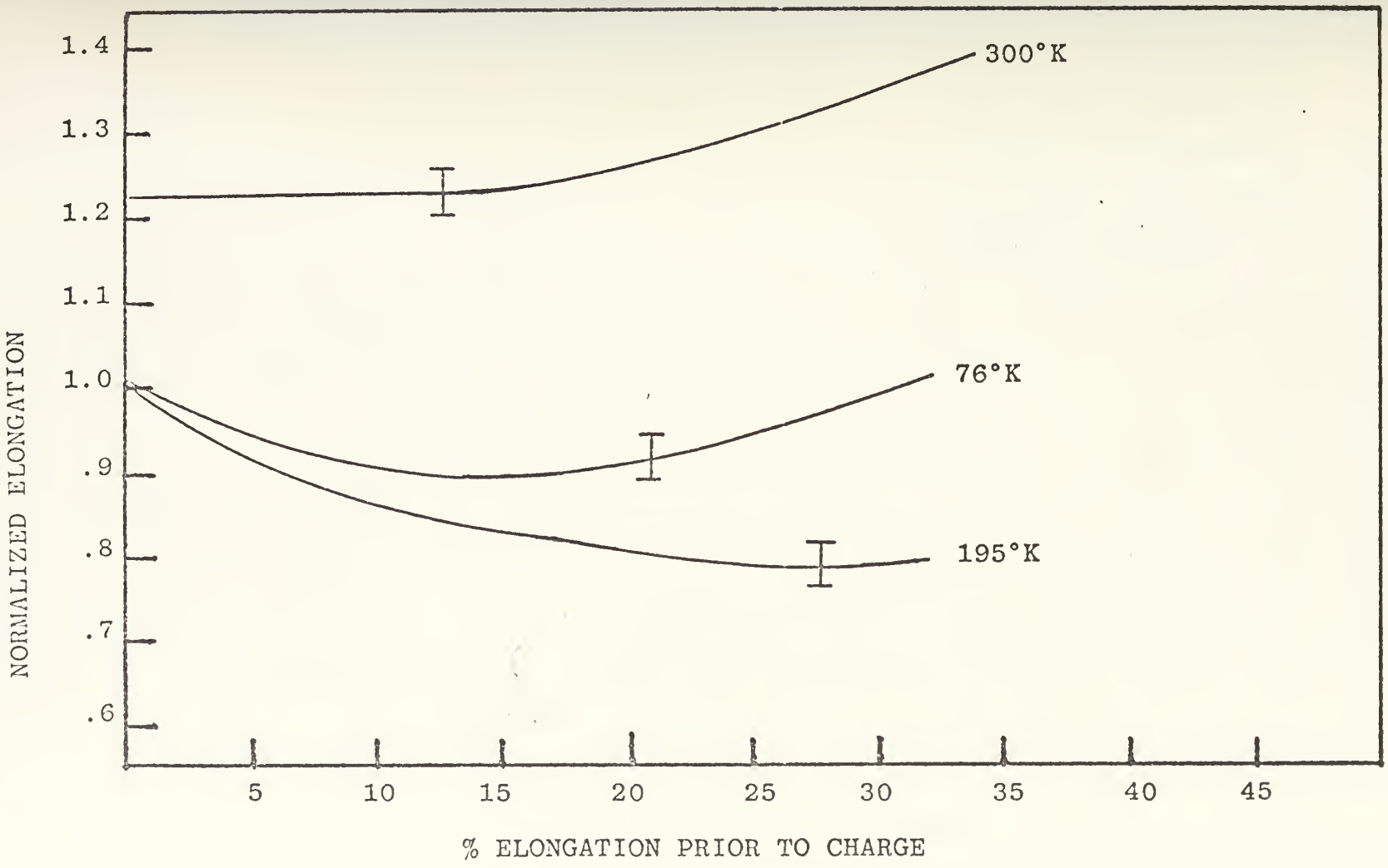

FIGURE 14. NORMALIZED ELONGATION VS PERCENT ELONGATION PRIOR TO CHARGE, UNNOTCHED, 21-6-9

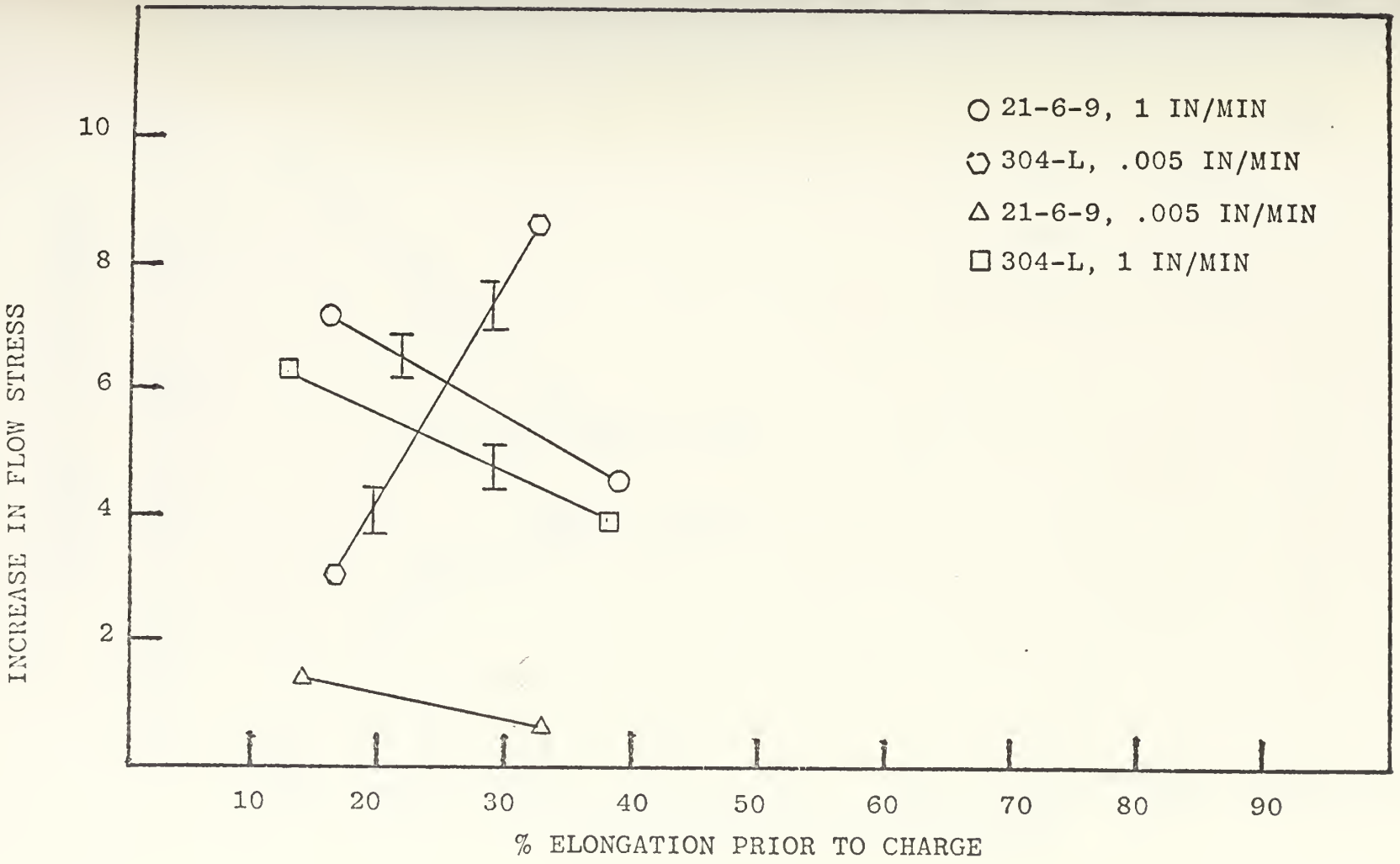

FIGURE 15. INCREASE IN FLOW STRESS VS PERCENT ELONGATION PRIOR TO CHARGE, 300°K

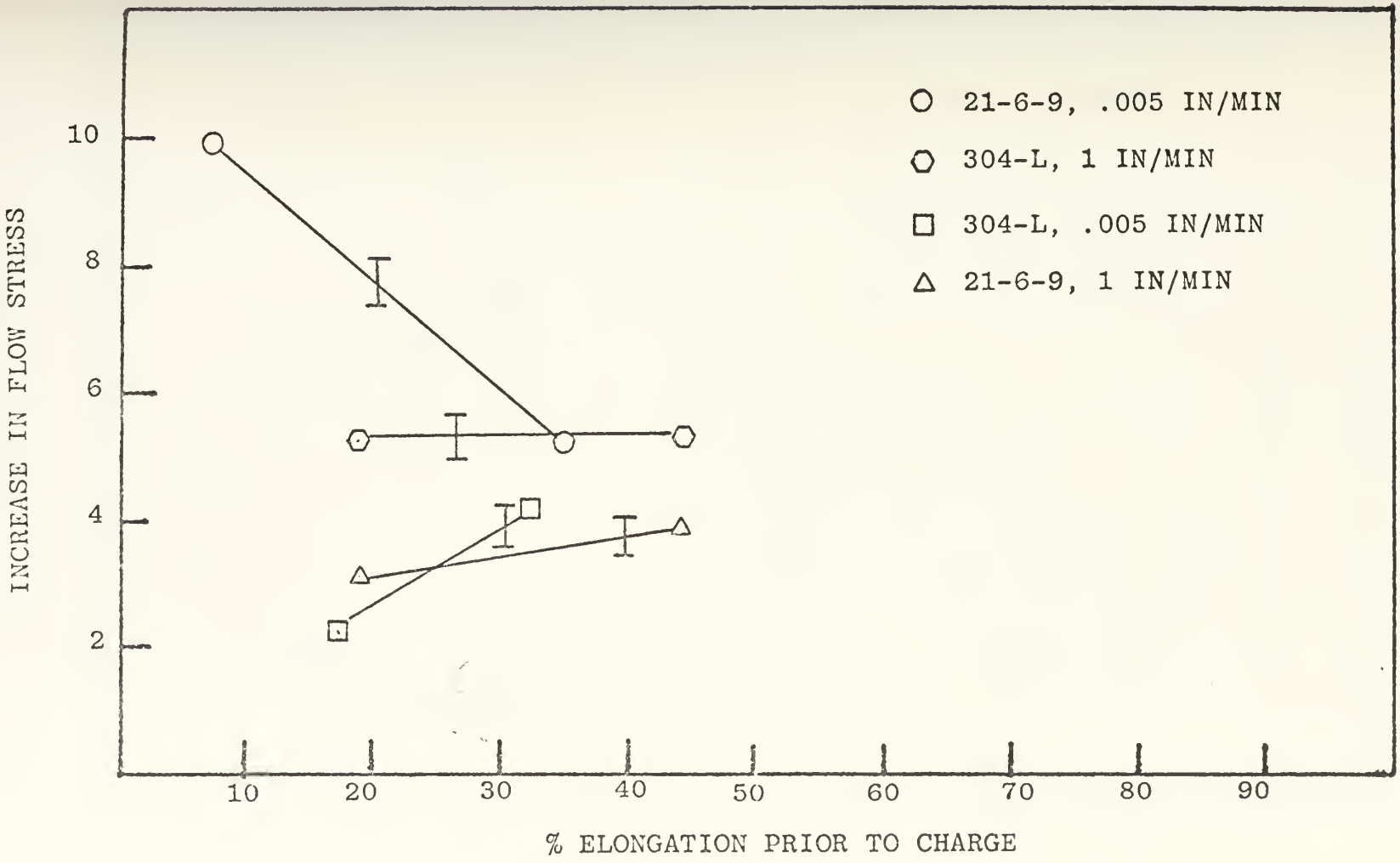

FIGURE 16. INCREASE IN FLOW STRESS VS PERCENT ELONGATION PRIOR TO CHARGE, 195°K

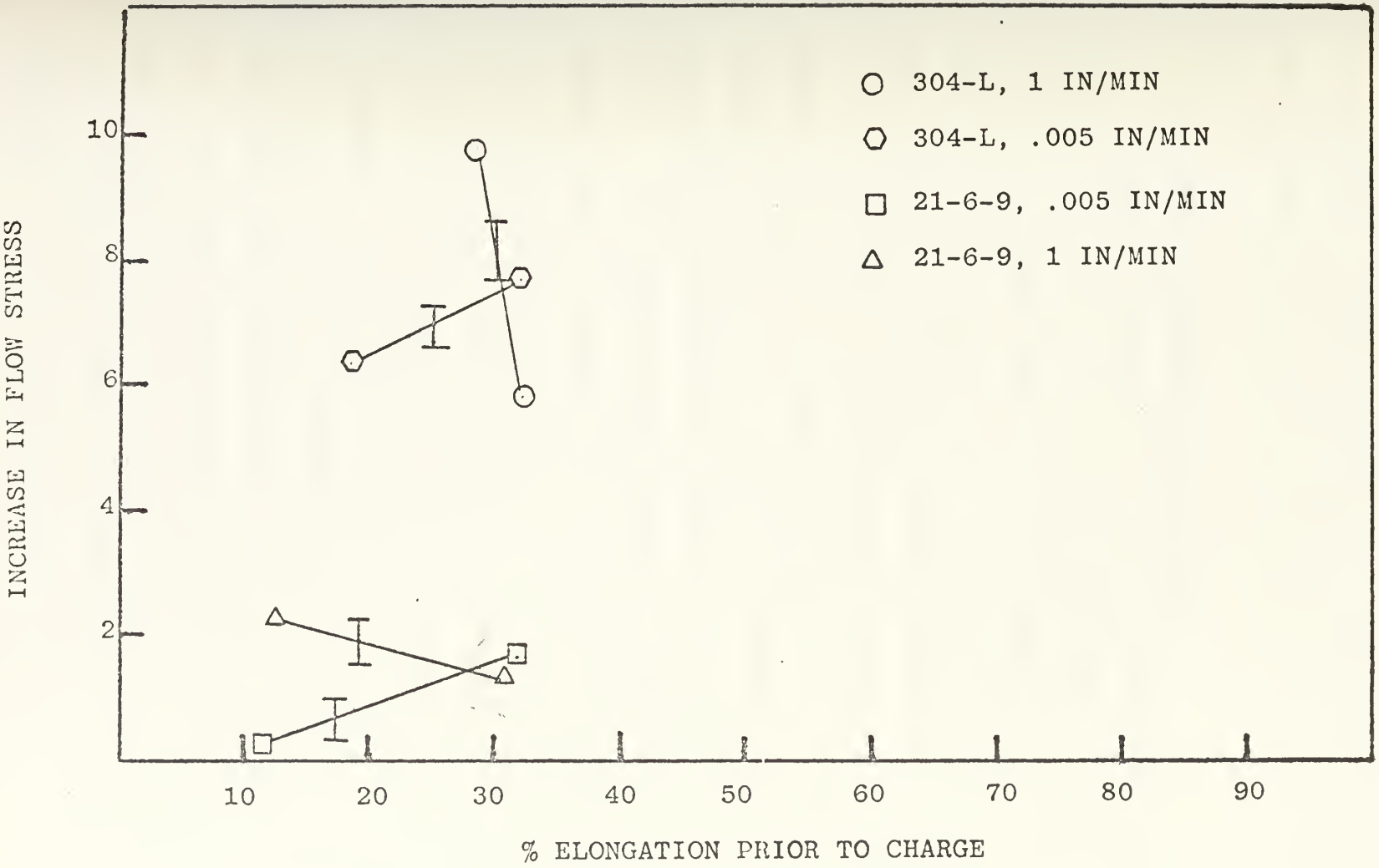

FIGURE 17. INCREASE IN FLOW STRESS VS PERCENT ELONGATION PRIOR TO CHARGE, 76°K

Analysis of Figures 13 and 14 indicates the effects that charging had on the specimens' normalized elongations, which are a measure of their ductility. These are correlated with the fractographic evidence compiled in part C of this section.

1. 304-L (Normalized Elongation)

Charging appeared to have a ductilizing effect on the charged 304-L specimens at 300°K and 195°K. However, this result is strongly affected by the baseline value of ductility used in the computations and sample machine differences. Fractographic evidence for charged and uncharged specimens at 300°K and 195°K (Figures 19, 20 and 23, 24) neither confirms or disputes any ductilizing effect. At 76°K (Figures 29 and 30) fractographic analysis confirms that a loss of ductility has occurred as indicated in Figure 13 for 0% pre-strain. For 300°K, 195°K and 76°K, (Figures 21, 25 and 29 respectively) fractographic interpretation lends credence to the graphical evidence (Figure 13) that a ductilizing effect occurred after charging the specimens which were pre-strained between 17 and 22 percent tensile elongation. The further increase in the normalized elongation at 300°K for 304-L at 35.6% pre-strain is substantiated by Figure 22. The corresponding loss in ductility at the two reduced temperatures of final pre-strains is correlated by Figures 26 and 30. An optical metallographic analysis of a 304-L specimen fractured at 76°K was conducted and is referred to in part D of this section.

2. 21-6-9 (Normalized Elongation)

The graphical results in Figure 14 for the charged 21-6-9 specimens with 0% pre-strain at 300°K, 195°K and 76°K are substantiated by fractographic figures 43, 44; 47, 48; and 51, 52 respectively. Further examination of Figure 14 indicates that a small amount of pre-strain followed by charging has an embrittling effect at reduced temperatures of 195°K and 76°K. Analysis of Figures 45, 49 and 53 at temperatures of 300°K, 195°K and 76°K agree with this fact. Continued elongation beyond 25% followed by charging appears fractographically to have a further embrittling effect. There is a reduction in dimple sizes and some quasi-cleavaging as indicated by Figures 50 and 54 for 195°K and 76°K. Graphically, however, this is not substantiated. For 300°K charging appears to reduce the dimple size as shown in Figures 43, 44, 45 and 46. The corresponding increase of ductility is indicated in Figure 14, however, it is not confirmed by the fractographic results.

The paradoxical results of an increase in ductility when cathodic charging is involved at the reduced temperatures of 300°K and 195°K may be explained by either of two possibilities. The first possibility is that of the solid solutioning softening phenomenon. Solute additions have been found by many observers to increase as well as decrease the low temperature strength in BCC metals, depending upon variables such as purity, temperature and strain rate. Its relevancy for FCC is unknown because all studies have been oriented

toward BCC structures which most readily accept interstitial or substitutional solutes. When there is a decrease in the strength of the alloys which are subjected to solute, this process is termed solution softening. Ravi and Gibala have proposed four mechanisms that might account for this effect. These include; scavenging, dislocation interaction at low temperatures, dislocation interstitial solute interactions at low temperatures causing a thermally activated deformation mechanism and alloy softening by substitutional solutes [20]. Tanaka believes that other factors in solid solution softening involve a decrease in activation energy, an increase ease in cross slipping, an increase in mobile dislocation density and changes in electronic configurations in parent alloys [21]. Although there has been conflicting reasons why this has occurred, it has been repeatly shown that oxygen atoms in solution with other residual interstitials in solution including hydrogen, nitrogen and carbon are the catalysts in the solid solutioning mechanism [22].

While the foregoing explanation of the solid solution softening mechanism is theoretically possible in FCC metals, it is considered that in the present case, all apparent "ductilizing" effects noted are more likely the result of variations in sample machining procedures from the baseline to charged samples. The occurrence of real softening effects due to charging is considered unlikely in view of the lack of previous reports of such phenomena in these well studied materials.

The results of the increase in flow stress vs. percent elongation prior to charging indicated that cathodic charging had the effect of increasing flow stress but conclusive evidence as to whether this increase was a result of hydrogen embrittlement and/or a martensitic transformation process could not be determined.

C. FRACTOGRAPHIC RESULTS

A comprehensive fractographic analysis was conducted on the fractured samples. Table II lists a compilation of the specimens which were studied under the Scanning Electron Microscope (SEM), Figure 18. Because it was felt that the most valid indications of embrittlement occurred at the low crosshead rate, these were the only specimens which were investigated. The SEM was used to study the total surface topography of the fractured specimen. Total material characterizations such as transgranular cleavage, quasi-cleavage, dimples formed by microvoid coalescence, tearing and fatigue striations can be studied utilizing this device. Each fractograph taken was chosen as the one most representative of the specimen's surface and the appropriate comment was made regarding its microstructural features. Any evidence of martensitic transformation or a possible embrittling trend will be alluded to in the analysis of each SEM fractograph.

D. DISCUSSION OF FRACTOGRAPHIC RESULTS

TABLE II. SCANNING ELECTRON MICROSCOPE FRACTOGRAPH INDEX

SEM NO	METAL	TEMPERATURE	% ELONG CHARGE	GEOM
2	304-L	300° K	0*	a
13	304-L	300° K	0	a
14	304-L	300° K	17.18	a
15	304-L	300° K	35.6	a
4	304-L	195° K	0*	a
18	304-L	195° K	0	a
19	304-L	195° K	17.97	a
20	304-L	195° K	31.25	a
6	304-L	76° K	0*	a
23	304-L	76° K	0	a
24	304-L	76° K	21.88	a
25	304-L	76° K	32.81	a
1	304-L	300° K	0*	b
16	304-L	300° K	0	b
17	304-L	300° K	7.8	b
17'	304-L	300° K	7.8	b
17"	304-L	300° K	7.8	b
3	304-L	195° K	0*	b
21	304-L	195° K	0	b
22	304-L	195° K	6.25	b
5	304-L	76° K	0*	b
26	304-L	76° K	0	b
26'	304-L	76° K	0	b
27	304-L	76° K	6.77	b
8	21-6-9	300° K	0*	a
28	21-6-9	300° K	0	a
29	21-6-9	300° K	14.84	a
30	21-6-9	300° K	33.75	a

* Denotes No Charge

TABLE II (Cont.)

SEM NO	METAL	TEMPERATURE	% ELONG CHARGE	GEOM
10	21-6-9	195°K	0*	a
33	21-6-9	195°K	0	a
34	21-6-9	195°K	10.93	a
35	21-6-9	195°K	34.38	a
12	21-6-9	76°K	0*	a
38	21-6-9	76°K	0	a
39	21-6-9	76°K	12.5	a
40	21-6-9	76°K	32.81	a
40'	21-6-9	76°K	32.81	a
7	21-6-9	300°K	0*	b
31	21-6-9	300°K	0	b
32	21-6-9	300°K	5.93	b
9	21-6-9	195°K	0*	b
36	21-6-9	195°K	0	b
37	21-6-9	195°K	4.68	b
11	21-6-9	76°K	0*	b
41	21-6-9	76°K	0	b
41'	21-6-9	76°K	0	b
42	21-6-9	76°K	2.34	b
42'	21-6-9	76°K	2.34	b
42"	21-6-9	76°K	2.34	b

* Denotes No Charge

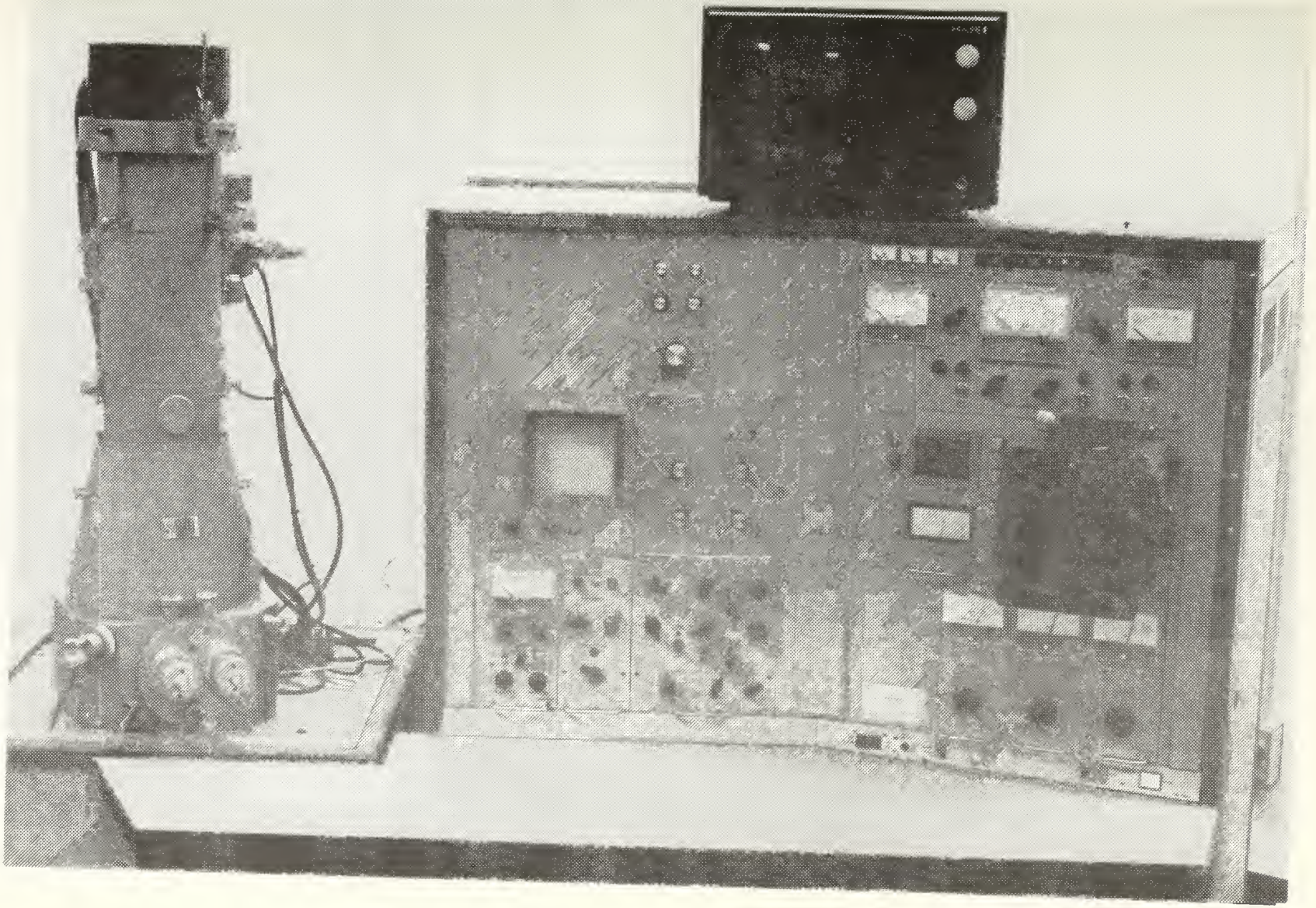

FIGURE 18. SCANNING ELECTRON MICROSCOPE (SEM)

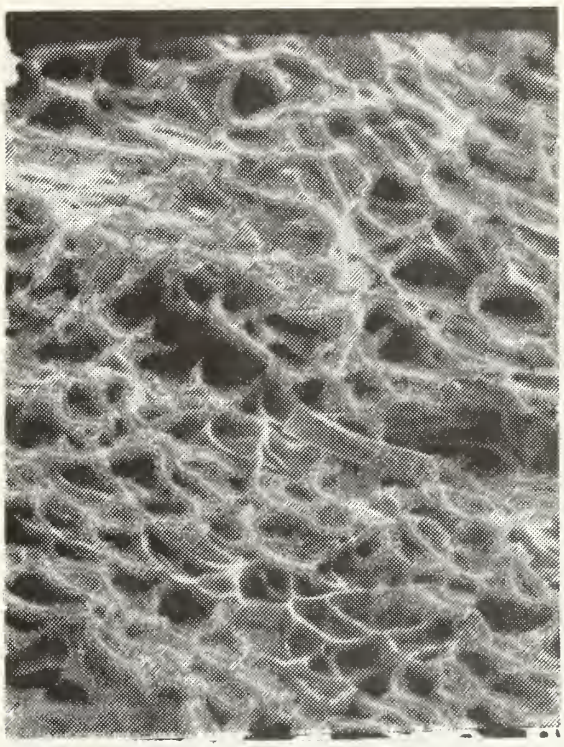

SEM FRACTOGRAPH 2 2400X

Uniformed dimples structure with some tear ridges indicates that tearing was probably the mechanism of local fracture. Slight pebbled substructure inside dimples is of unknown origin.

FIGURE 19. 304-L, 300°K, UNNOTCHED, UNCHARGED

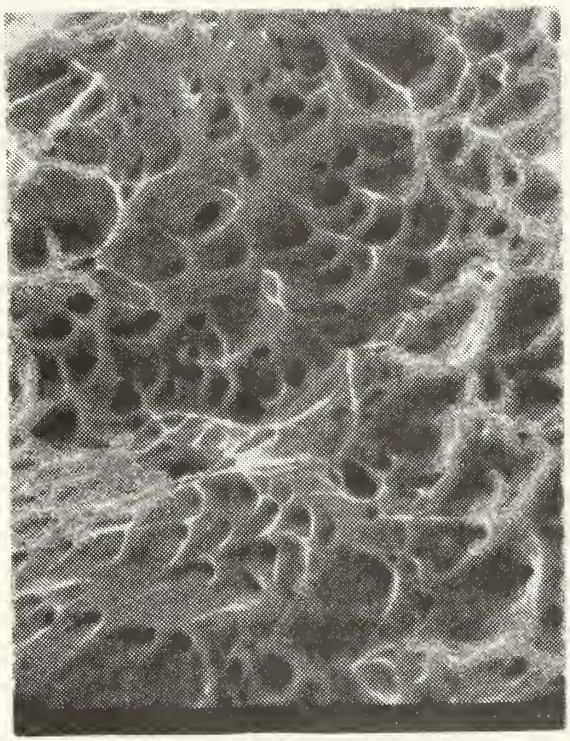

SEM FRACTOGRAPH 13 2400X

Elongated shear dimples indicate minor stretching. Bright contrast on dimple rims could have resulted from minor tearing.

FIGURE 20. 304-L, 300°K, UNNOTCHED,
0% ELONGATION PRIOR TO CHARGE

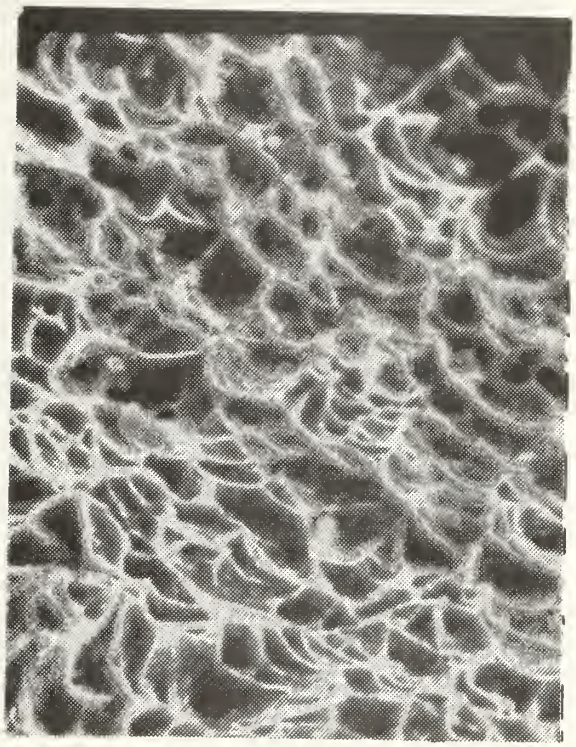

SEM FRACTOGRAPH 14 2500X

Uniformed dimples fracture surface with minor tearing and stretching.

FIGURE 21. 304-L, 300°K, UNNOTCHED, 17.18% ELONGATION PRIOR TO CHARGE

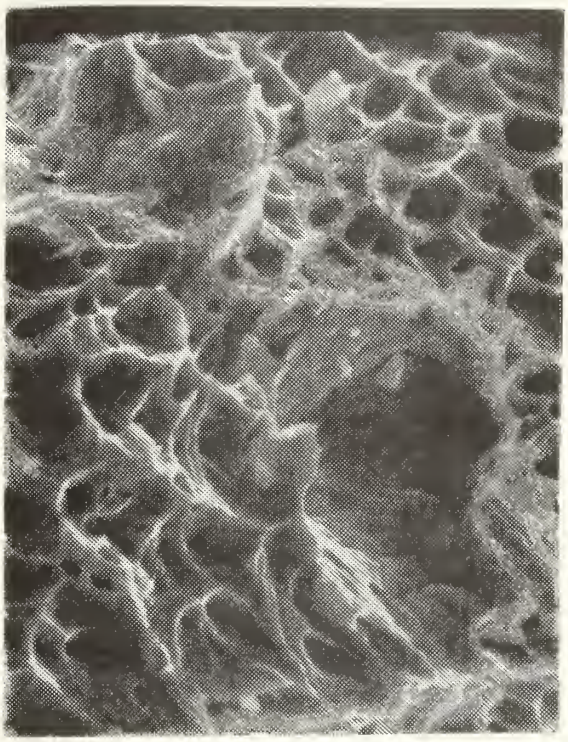

SEM FRACTOGRAPH 15 2500X

Slight elongation of dimples with formation of tear ridges which has produced a bright contrast in the SEM image. Non-spherical, non-metallic inclusions are scattered among a pebbled substructure.

FIGURE 22. 304-L, 300°K, UNNOTCHED, 35.6% ELONGATION PRIOR TO CHARGE

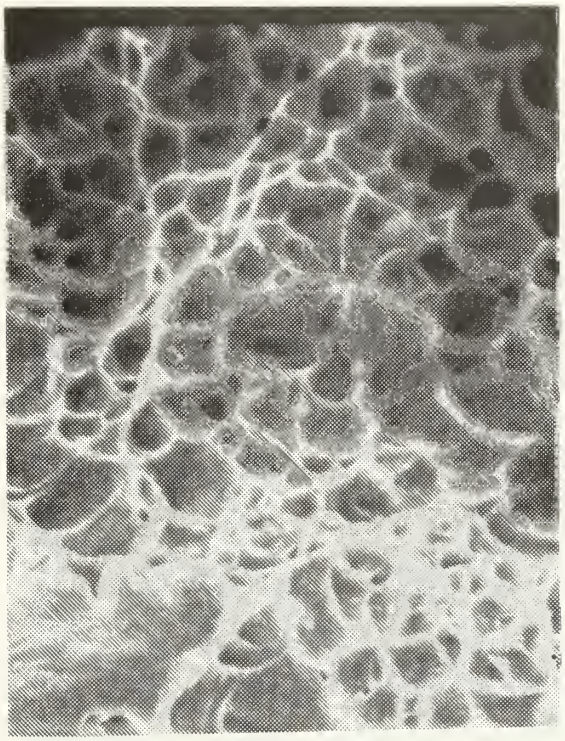

SEM FRACTOGRAPH 4 2350X

Uniform dimple structures with slightly rounder bottoms than previous dimples. Minor tearing and pebbling apparent.

FIGURE 23. 304-L, 195°K, UNNOTCHED, UNCHARGED

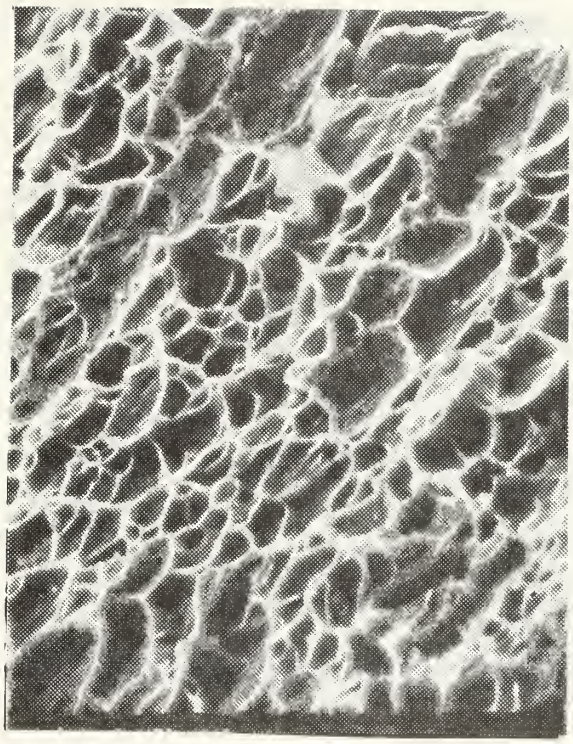

SEM FRACTOGRAPH 18 2500X

Uniformally dimples structure with indications of minor tearing, stretching and pebbling.

FIGURE 24. 304-L, 195°K, UNNOTCHED, 0% ELONGATION PRIOR TO CHARGE

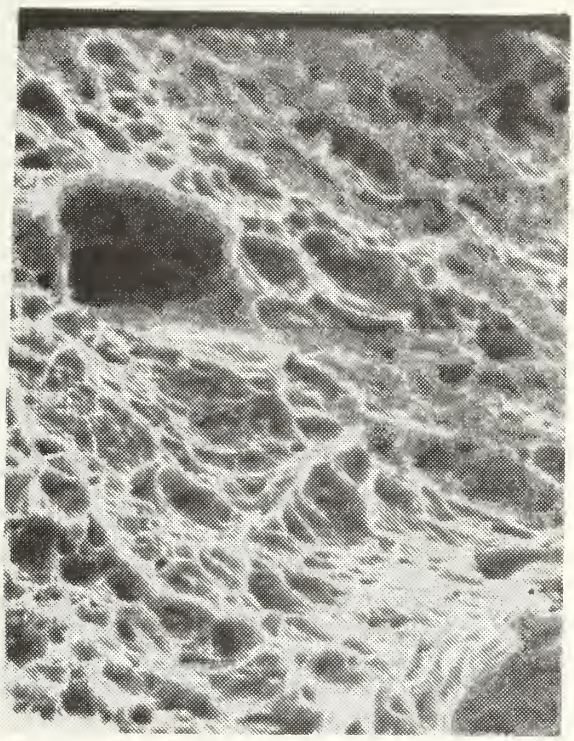

SEM FRACTOGRAPH 19 2400X

A non-uniformally dimpled structure is contrasted brightly by a tearing mechanism.

FIGURE 25. 304-L, 195°K, UNNOTCHED, 17.97% ELONGATION PRIOR TO CHARGE

SEM FRACTOGRAPH 20 2400X

Large elongated dimples contrasted brightly by the tear ridges. Uniform pebbled substructure dominates the internal floors of the dimples.

FIGURE 26. 304-L, 195°K, UNNOTCHED, 31.25% ELONGATION PRIOR TO CHARGE

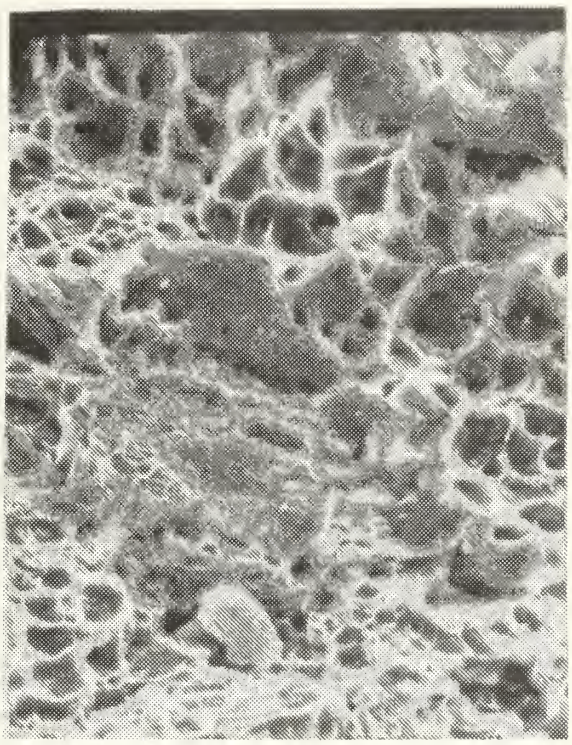

SEM FRACTOGRAPH 6 2300X

Non-uniform dimples with a small amount of quasi-cleavage. Cleavage usually occurs in body-centered-cubic metals indicating that a martensitic structure may have occurred. Light microscopy confirms a martensitic structure near fracture surface, apparently strain-induced -- not temperature-induced.

FIGURE 27. 304-L, 76°K, UNNOTCHED, UNCHARGED

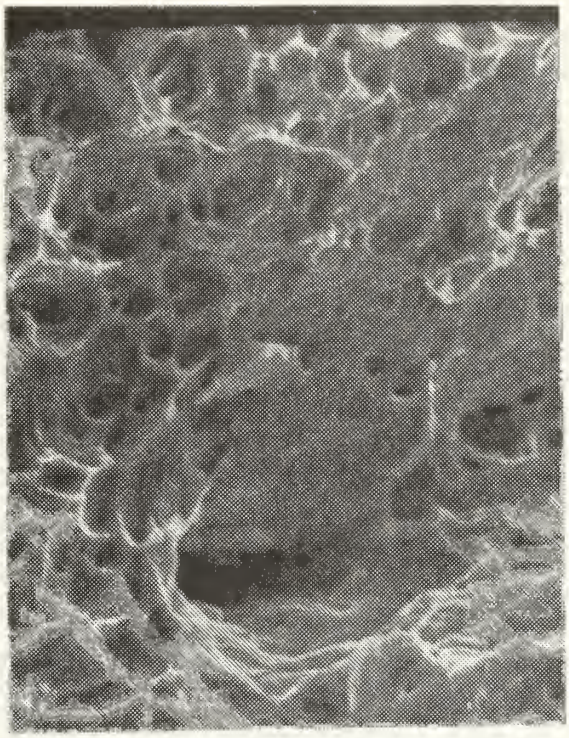

SEM FRACTOGRAPH 23 2350X

Large microvoid surrounded by non-uniformed dimples. Microvoids are initiated at interfaces between the matrix and particles such as carbides, precipitates and inclusions, and also at imperfections such as microporosity and microcracks. Some evidence of minor pebbling with non-metallic inclusions.

FIGURE 28. 304-L, 76°K, UNNOTCHED, 0% ELONGATION PRIOR TO CHARGE

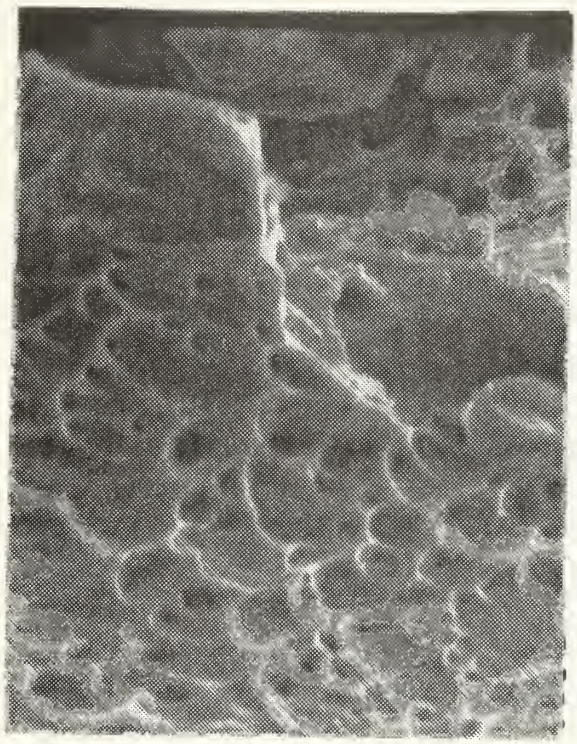

SEM FRACTOGRAPH 24 2400X

Elongated shear dimples with some evidence of quasi-cleavage. This usually appears when poorly defined cleavage facets are connected by tear ridges and shallow dimples occur. The possibility of martensite was confirmed subsequently by light microscopy.

FIGURE 29. 304-L, 76°K, UNNOTCHED, 21.88% ELONGATION PRIOR TO CHARGE

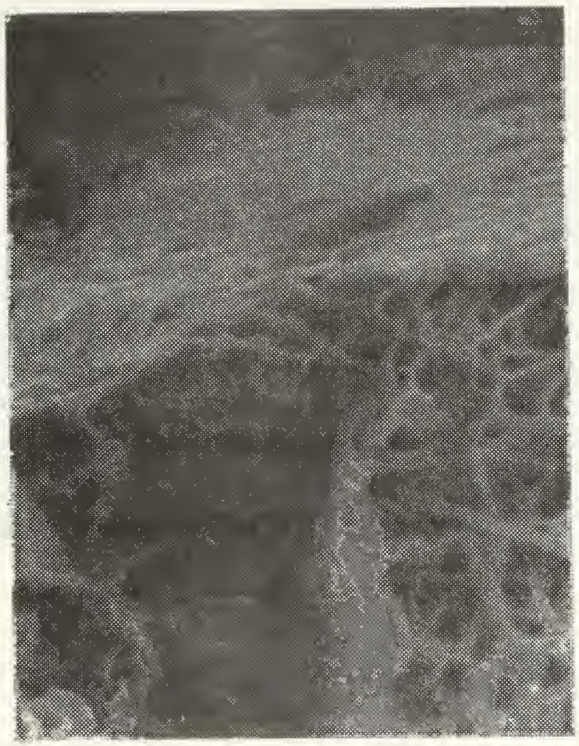

SEM FRACTOGRAPH 25 2400X

Upper area is indicative of stretching while lower area is dimpled. There is a small amount of fragmentation left of the dimple area.

FIGURE 30. 304-L, 76°K, UNNOTCHED, 32.81% ELONGATION PRIOR TO CHARGE

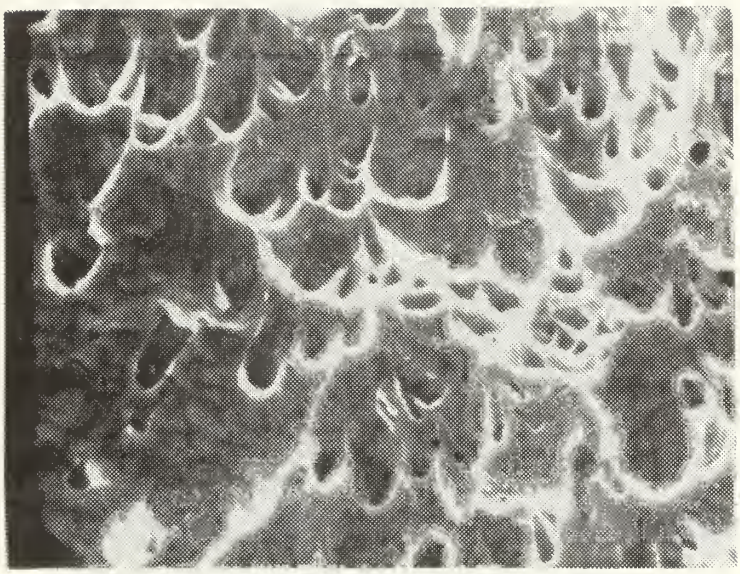

SEM FRACTOGRAPH 1 2300X

Slight elongation of dimples indicates either ductile tearing and/or the existence of shear dimples. In the former case it would be caused by a non-axial stress condition and is indicative that tensile tearing is not the predominant mechanism of fracture. Shear dimples occur usually in the shear lip zone. Pebbled substructure is of an unknown origin.

FIGURE 31. 304-L, 300°K, NOTCHED, UNCHARGED

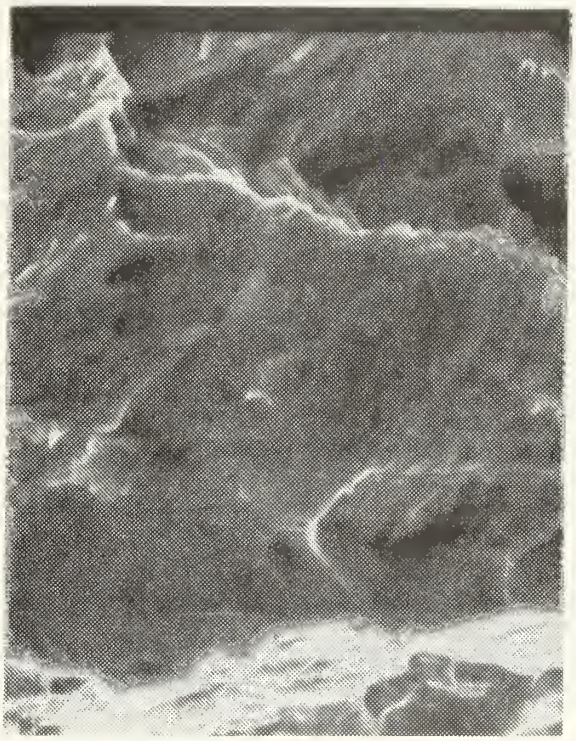

SEM FRACTOGRAPH 16 2600X

Predominantly-pebbled structure with some plate-like faceting.

FIGURE 32. 304-L, 300°K, NOTCHED, 0% ELONGATION PRIOR TO CHARGE

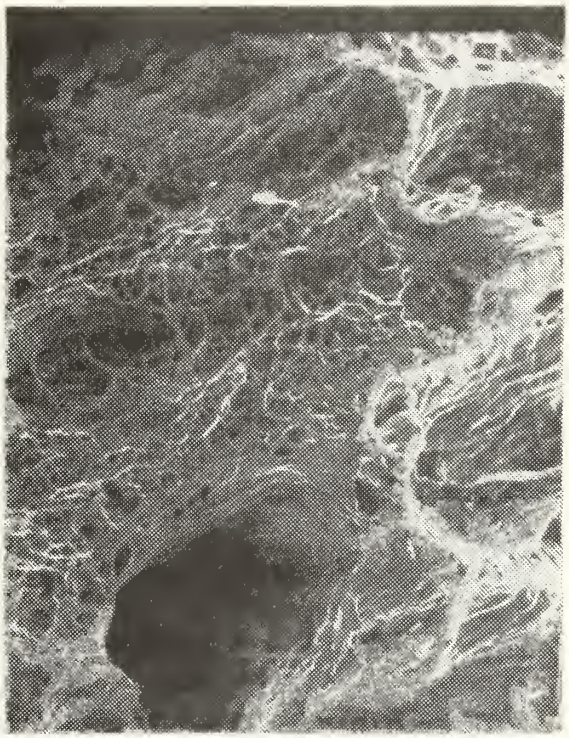

SEM FRACTOGRAPH 17 630X

Large microvoid formation within a fibrous dimpled network. Inclusions are evident even at low magnification.

FIGURE 33. 304-L, 300°K, NOTCHED, 7.8% ELONGATION PRIOR TO CHARGE

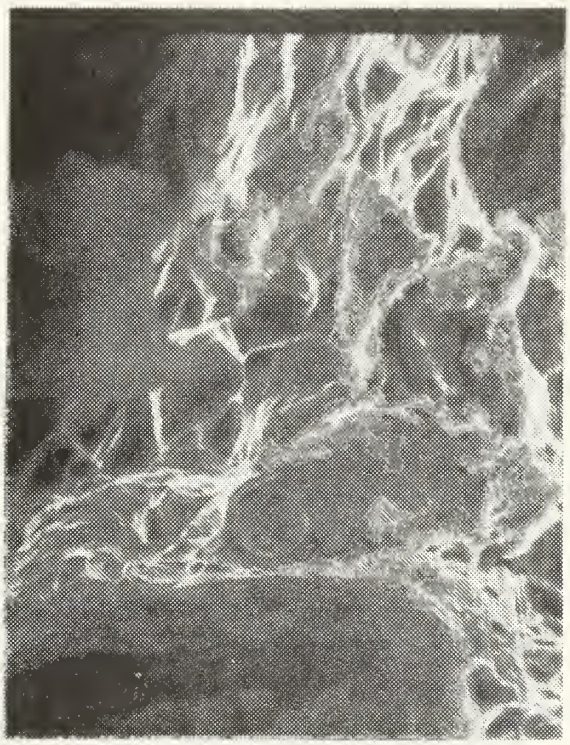

SEM FRACTOGRAPH 17' 2500X

Magnified inclusion with a dimple adjacent to a large microvoid. Globular inclusion is probably a result in the formation of microvoids and is a precipitate of the parent metal.

FIGURE 34. 304-L, 300°K, NOTCHED, 7.8% ELONGATION PRIOR TO CHARGE

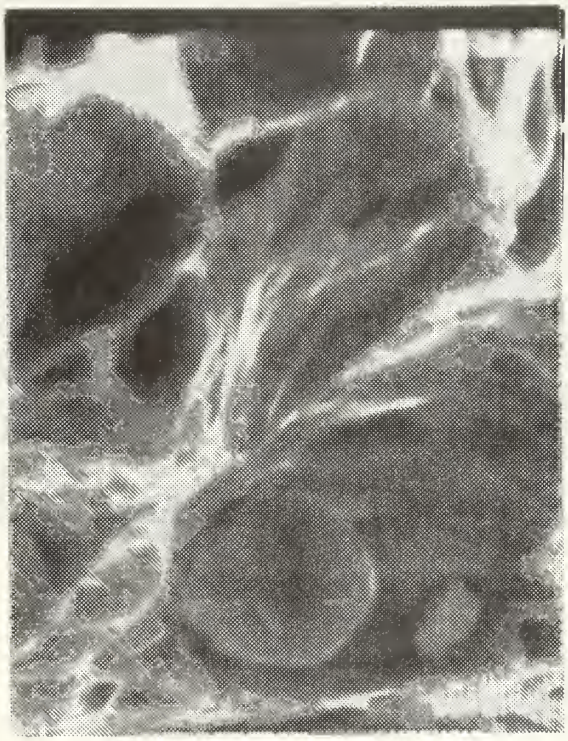

SEM FRACTOGRAPH 17" 6500X

Highest magnification before loss of resolution of the globular inclusion. In this specimen inclusions were noted not only on the dimple crater but also attached to the micro-void walls.

FIGURE 35. 304-L, 300°K, NOTCHED, 7.8% ELONGATION PRIOR TO CHARGE

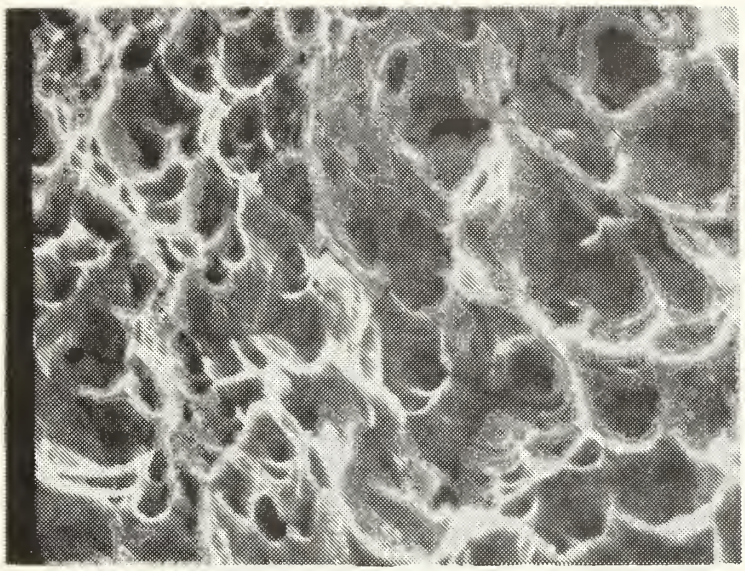

SEM FRACTOGRAPH 3 2300X

Non-uniformed dimples with tear ridges contrasted brightly. Slight stretching noted with pebbled substructure predominating the internal dimple areas.

FIGURE 36. 304-L, 195°K, NOTCHED, UNCHARGED

SEM FRACTOGRAPH 21 2400X

Pronounced shear dimples associated with stretching.

FIGURE 37. 304-L, 195°K, NOTCHED, 0% ELONGATION PRIOR TO CHARGE

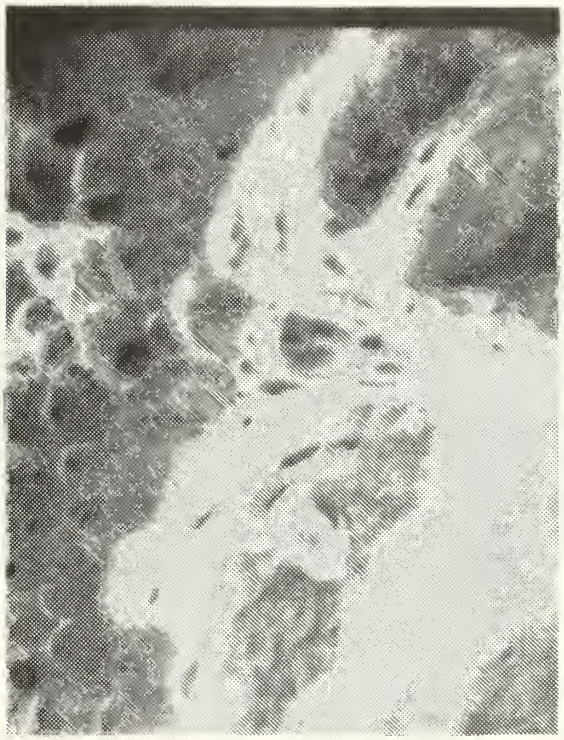

SEM FRACTOGRAPH 22 2400X

Shear dimples with minor stretching and tearing indicated.

FIGURE 38. 304-L, 195°K, NOTCHED, 6.25% ELONGATION PRIOR TO CHARGE

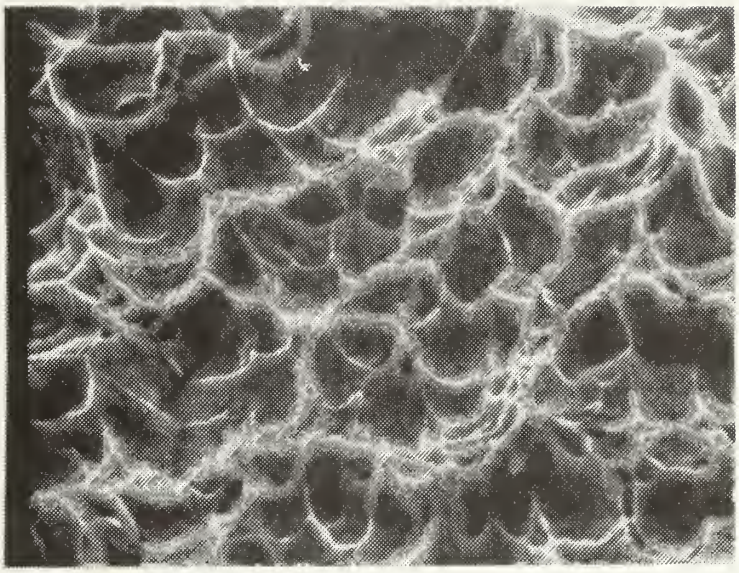

SEM FRACTOGRAPH 5 2400X

Uniformed dimples slightly elongated indicating that minor tearing and stretching has occurred. Pebbling is noted in the substructure.

FIGURE 39. 304-L, 76°K, NOTCHED, UNCHARGED

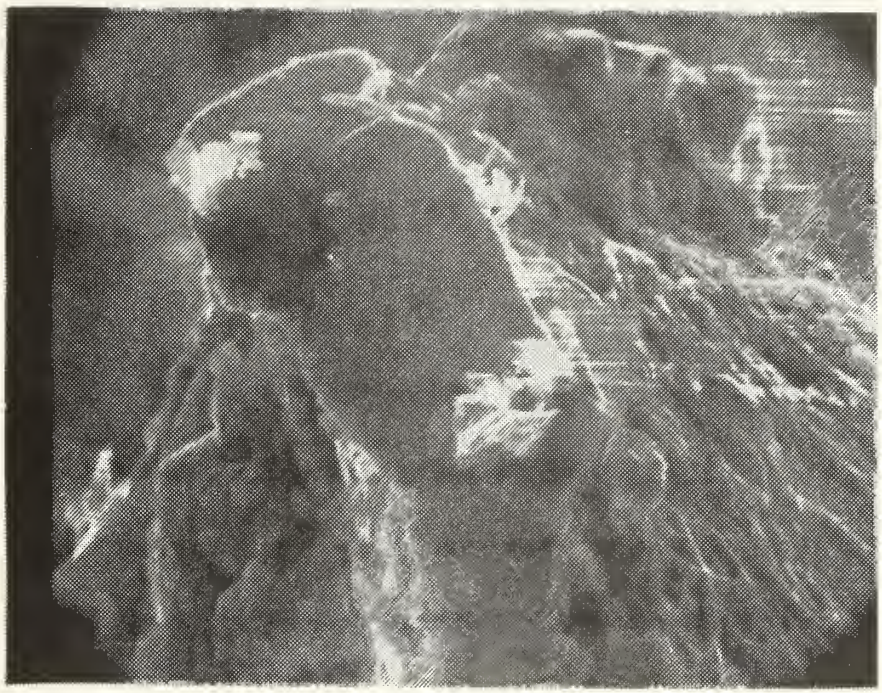

SEM FRACTOGRAPH 26 2500X

Center structure gives appearance of quasi-cleavage but fracture surface may have been damaged during fracture.

FIGURE 40. 304-L, 76°K, NOTCHED, 0% ELONGATION PRIOR TO CHARGE

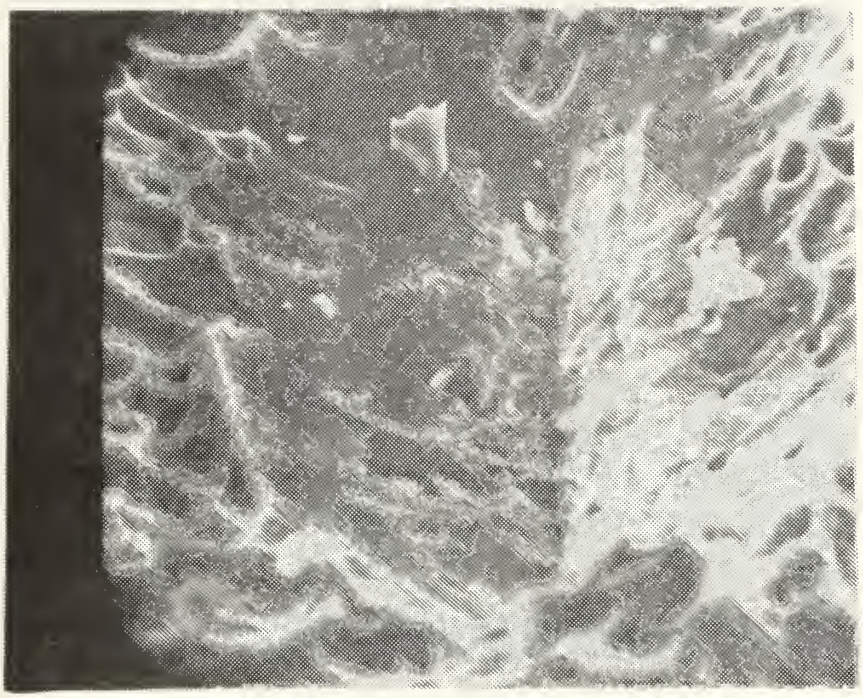

SEM FRACTOGRAPH 26' 2400X

Another view of same specimen showing stretching in the bottom of a V-shaped trough surrounded by shear dimples. Numerous non-metallic inclusions are evident within the stretched trough.

FIGURE 41. 304-L, 76°K, NOTCHED, 0% ELONGATION PRIOR TO CHARGE

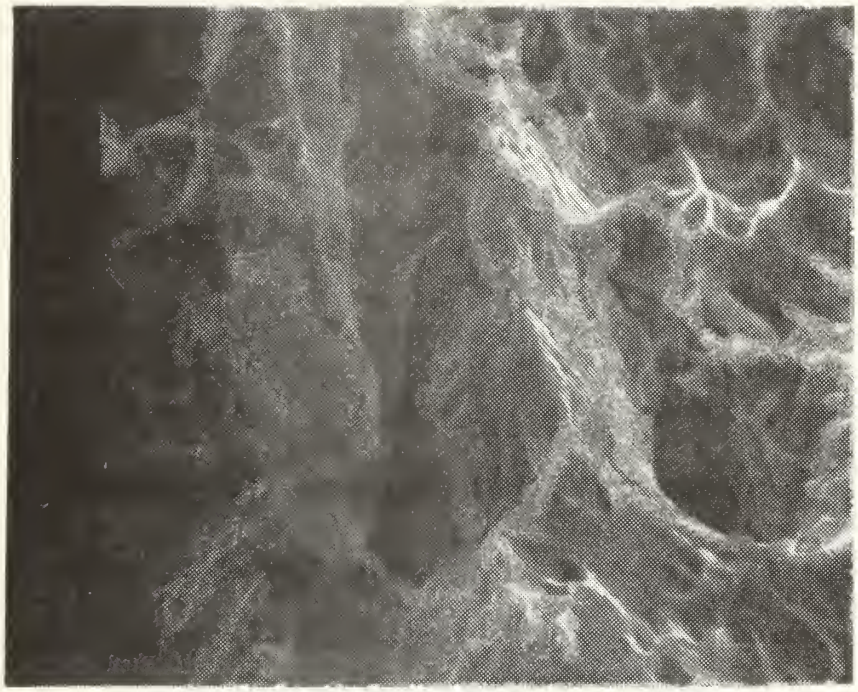

SEM FRACTOGRAPH 27 2500X

Large microvoids with irregular inclusions. Shear and/or tear dimples surround void. Internal walls of void have some pebbled structure with non-metallic inclusions of spherical and non-spherical geometries.

FIGURE 42. 304-L, 76°K, NOTCHED, 6.77% ELONGATION PRIOR TO CHARGE

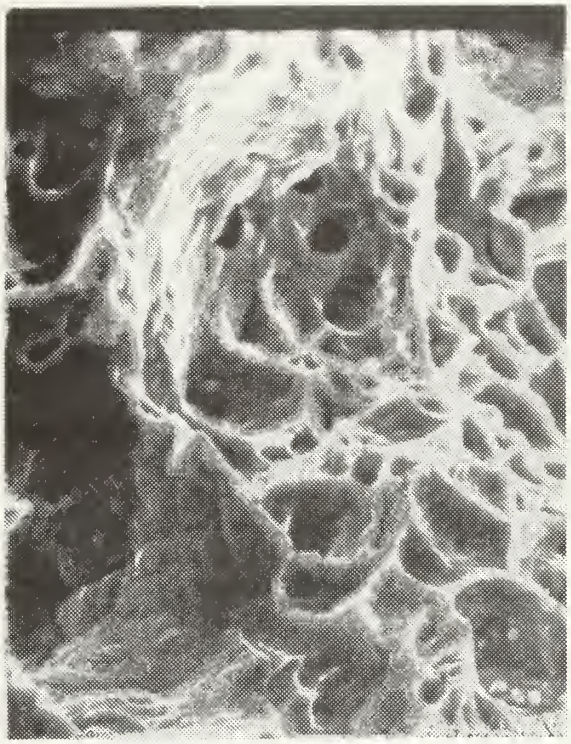

SEM FRACTOGRAPH 8 2550X

Non-uniformed dimpled structure with minor microvoids.

Pebbled structure predominates within the dimpled areas.

Squarish inclusions are noted within the microvoids.

FIGURE 43. 21-6-9, 300°K, UNNOTCHED, UNCHARGED

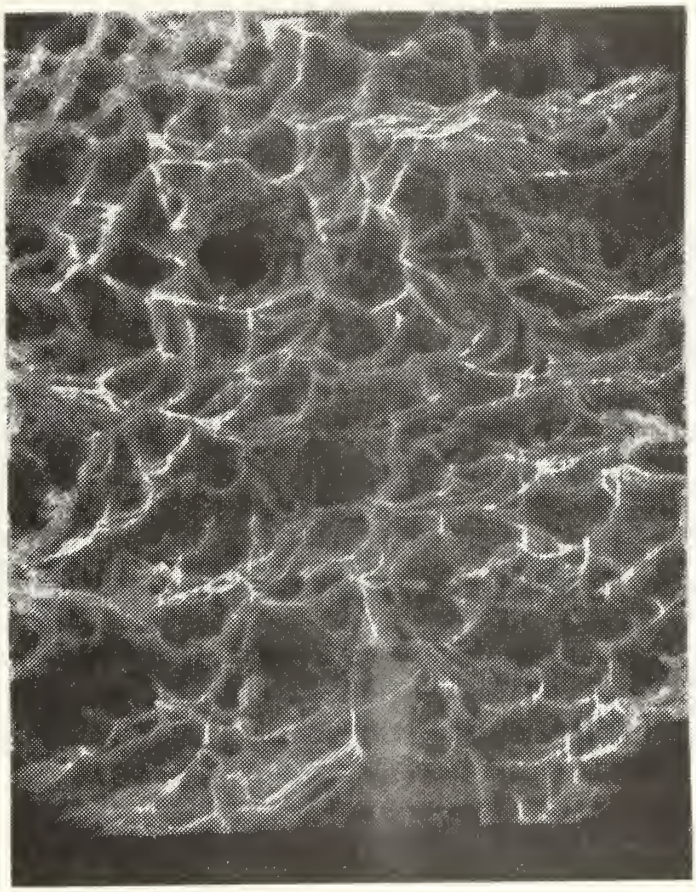

SEM FRACTOGRAPH 28 2300X

Uniformed dimpled structure predominates fracture surface. Pebbling is noted inside dimples with some slight tearing indicated.

FIGURE 44. 21-6-9, 300°K, UNNOTCHED, 0% ELONGATION PRIOR TO CHARGE

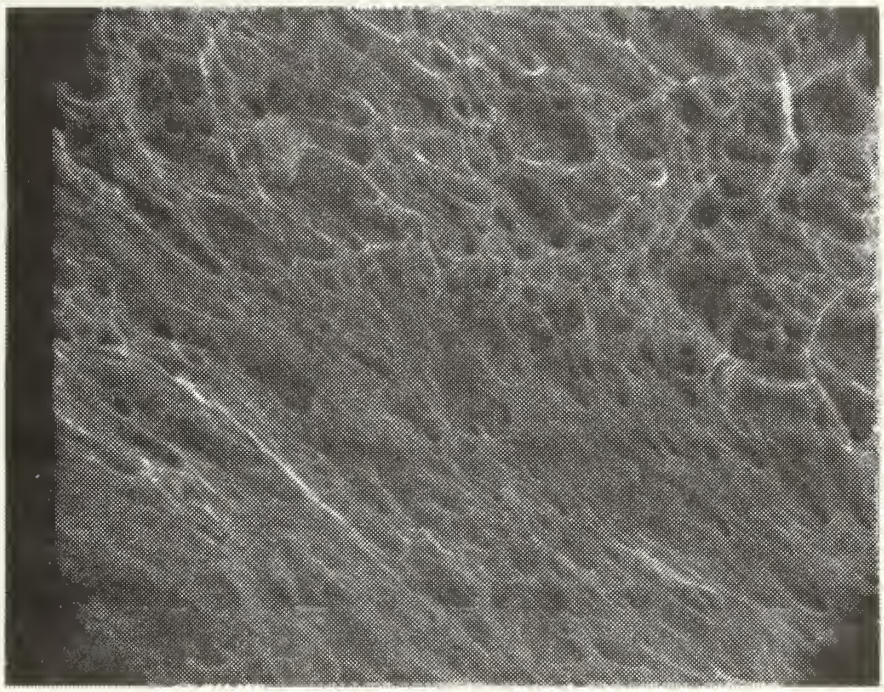

SEM FRACTOGRAPH 29 2400X

Adjacent areas of shear dimples and stretching indicated.

FIGURE 45. 21-6-9, 300°K, UNNOTCHED, 14.84% ELONGATION PRIOR TO CHARGE

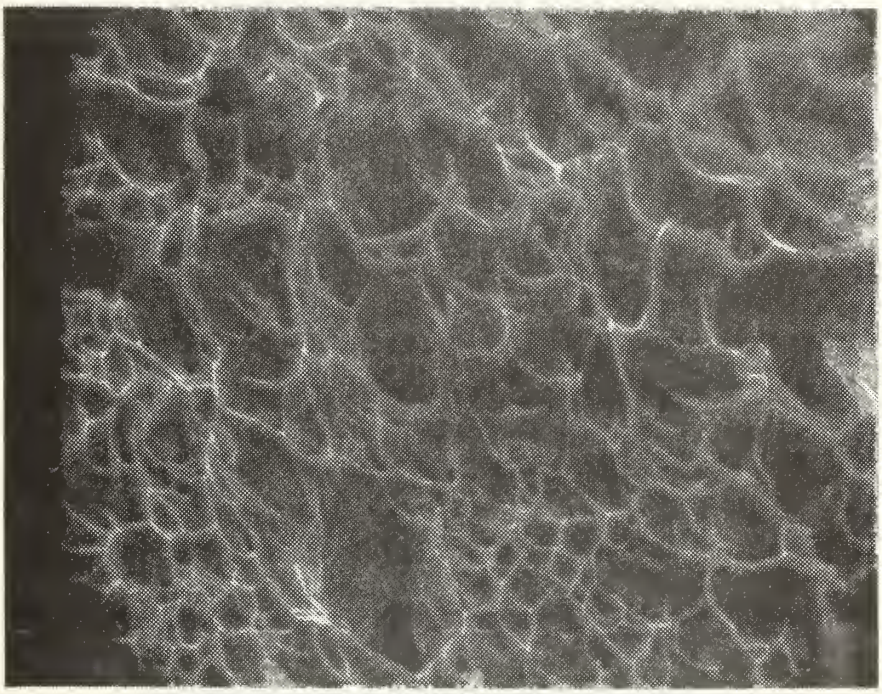

SEM FRACTOGRAPH 30 2300X

Slightly elongated dimples surrounding small microvoid formations. Pebbled substructure occurs within the voids with minor stretching and tearing indicated.

FIGURE 46. 21-6-9, 300°K, UNNOTCHED, 33.75% ELONGATION PRIOR TO CHARGE

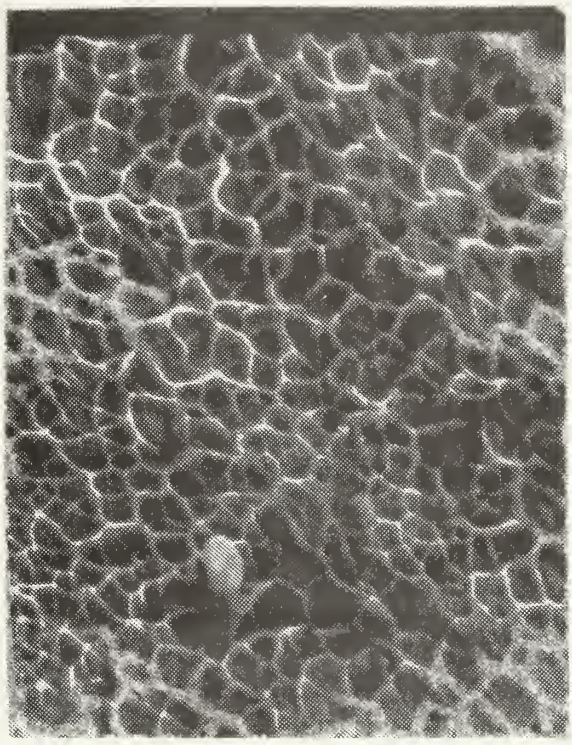

SEM FRACTOGRAPH 10 2300X

Minor elongation of uniform dimples. Pebbling predominates the substructure of the dimples.

FIGURE 49. 21-6-9, 195°K, UNNOTCHED, UNCHARGED

SEM FRACTOGRAPH 33 2400X

Non-unform dimples with minor tear ridges. There are some indications that possible quasi-cleavage has occurred on the tear ridges.

FIGURE 48. 21-6-9, 195°K, UNNOTCHED, 0% ELONGATION PRIOR TO CHARGE

SEM FRACTOGRAPH 34 2300X

Non-uniformed dimpled fracture surface with minor tearing and/or quasi-cleavaging occurring.

FIGURE 49. 21-6-9, 195°K, UNNOTCHED, 10.93% ELONGATION PRIOR TO CHARGE

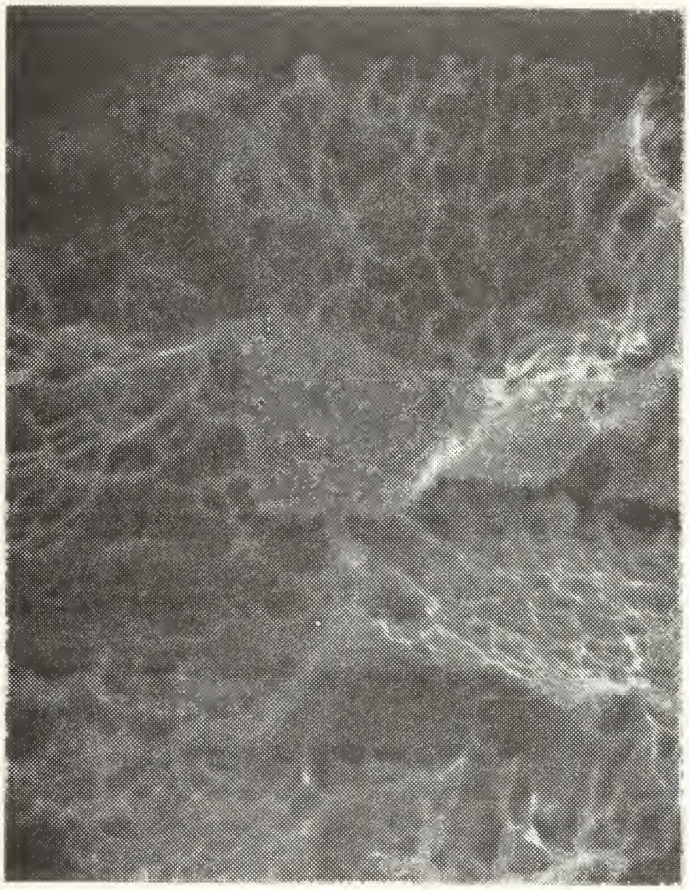

SEM FRACTOGRAPH 35 2300X

Non-uniformed dimples with some evidence of quasi-cleavaging and stretching occurring.

FIGURE 50. 21-6-9, 195°K, UNNOTCHED, 34.38% ELONGATION PRIOR TO CHARGE

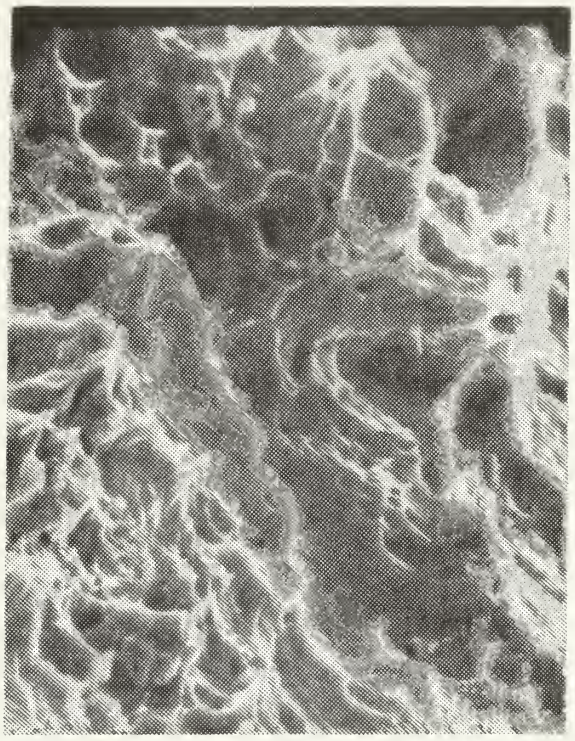

SEM FRACTOGRAPH 12 2400X

Mixture of dimples and regions of slight tearing may be the result of cleavage. Bright contrast is due to tearing.

FIGURE 51. 21-6-9, 76°K, UNNOTCHED, UNCHARGED

SEM FRACTOGRAPH 38 2400X

Non-uniformed dimples with minor tearing and stretching.

Possible evidence of quasi-cleavage.

FIGURE 52. 21-6-9, 76°K, UNNOTCHED, 0% ELONGATION PRIOR TO CHARGE

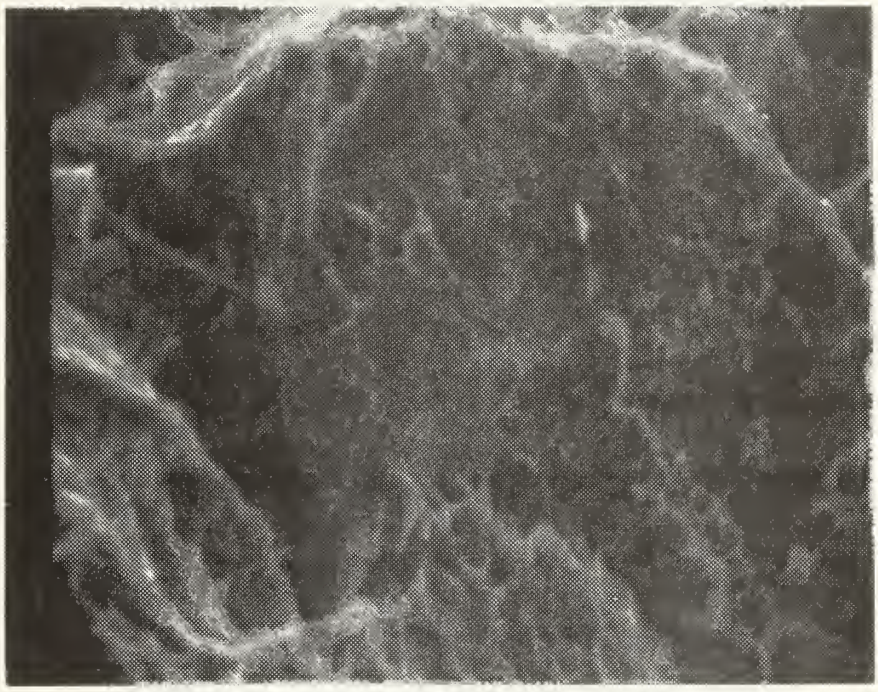

SEM FRACTOGRAPH 39 2400X

Non-uniformed dimples possibly resulting from stretching and/or tearing. Slight pebbled appearance may be quasi-cleavage or microfaceting. Inclusions are noted within the substructure.

FIGURE 53. 21-6-9, 76°K, UNNOTCHED, 12.5% ELONGATION PRIOR TO CHARGE

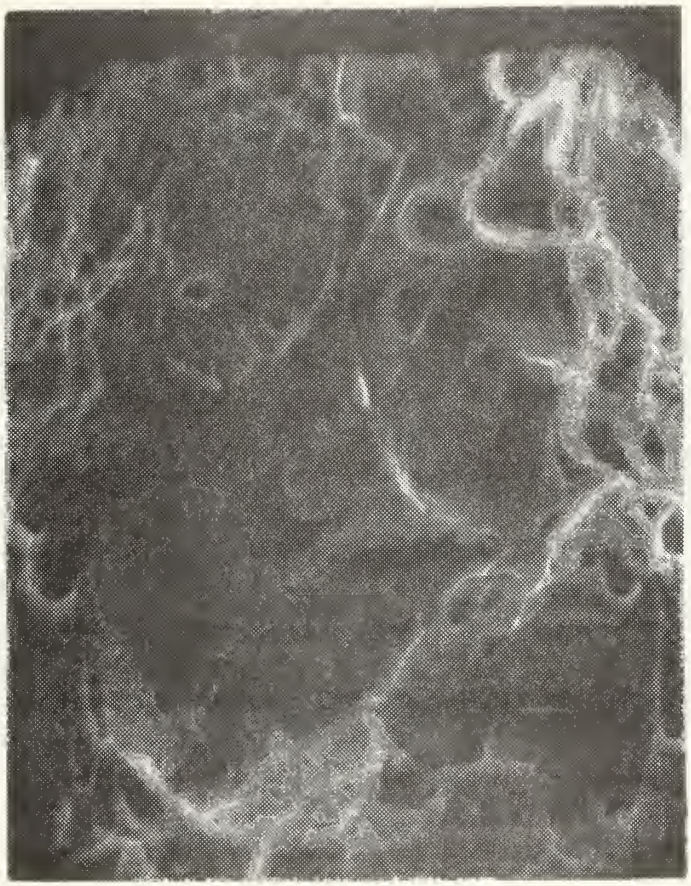

SEM FRACTOGRAPH 40 2300X

Stretched areas and distinctly pebbled areas indicative of possible quasi-cleavage. Higher magnification shows definite evidence of cleavage facets.

FIGURE 54. 21-6-9, 76°K, UNNOTCHED, 32.81% ELONGATION PRIOR TO CHARGE

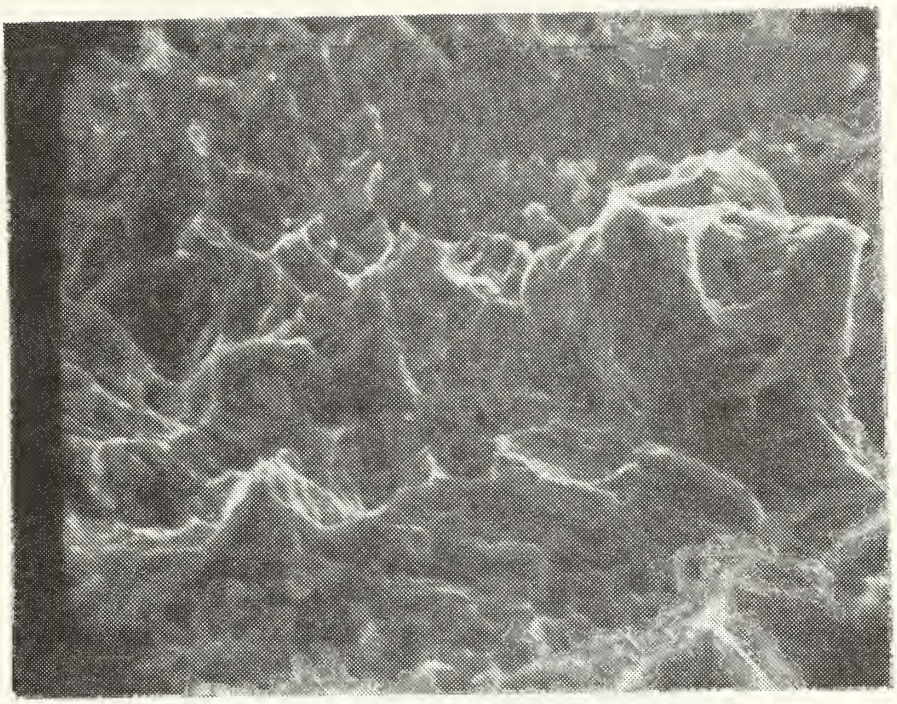

SEM FRACTOGRAPH 40' 2200X

Definite cleavage facets with pronounced tearing ridges evident.

FIGURE 55. 21-6-9, 76°K, UNNOTCHED, 32.81% ELONGATION PRIOR TO CHARGE

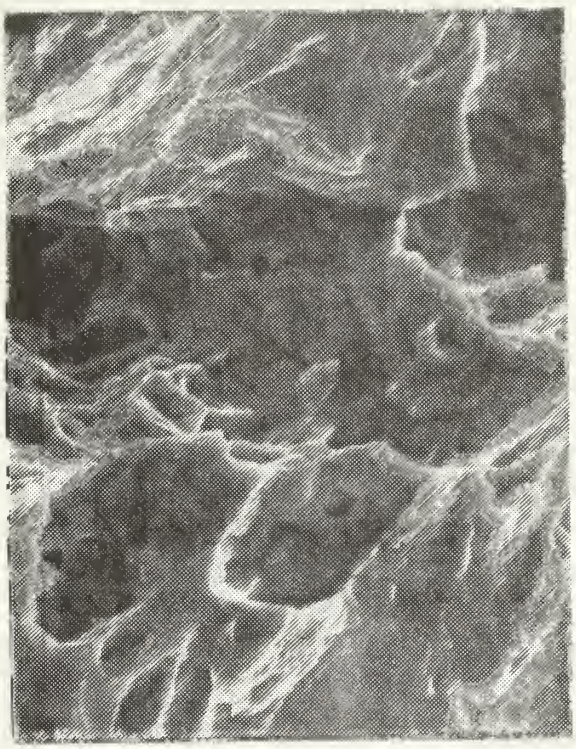

SEM FRACTOGRAPH 7 2400X

Almost complete absence of dimples. High degree of tearing or microcleavage. Extremely minor microvoid formation. This sample has a completely pebbled substructure within the zones of tearing, apparently associated with the micro-cleavage.

FIGURE 56. 21-6-9, 300°K, NOTCHED, UNCHARGED

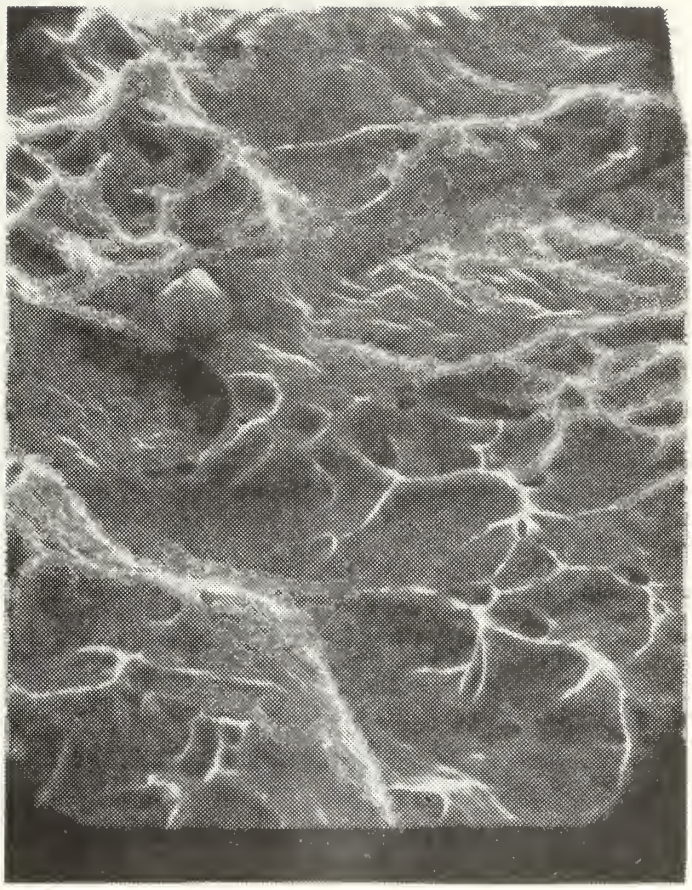

SEM FRACTOGRAPH 31 2350X

Tear ridges coupled with shear dimples in a predominantly pebbled substructure. Minor stretching noted.

FIGURE 59. 21-6-9, 300°K, NOTCHED, 0% ELONGATION PRIOR TO CHARGE

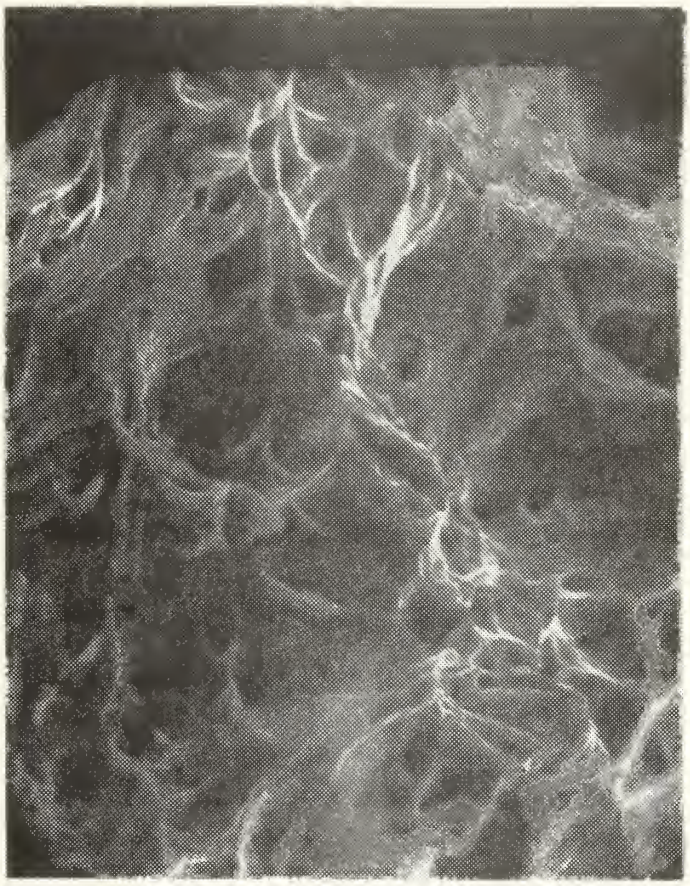

SEM FRACTOGRAPH 32 2400X

Tear ridges within a moderately pebbled structure. Minor microvoid formation surrounded by indications of stretching.

FIGURE 58. 21-6-9, 300°K, NOTCHED, 5.93% ELONGATION PRIOR TO CHARGE

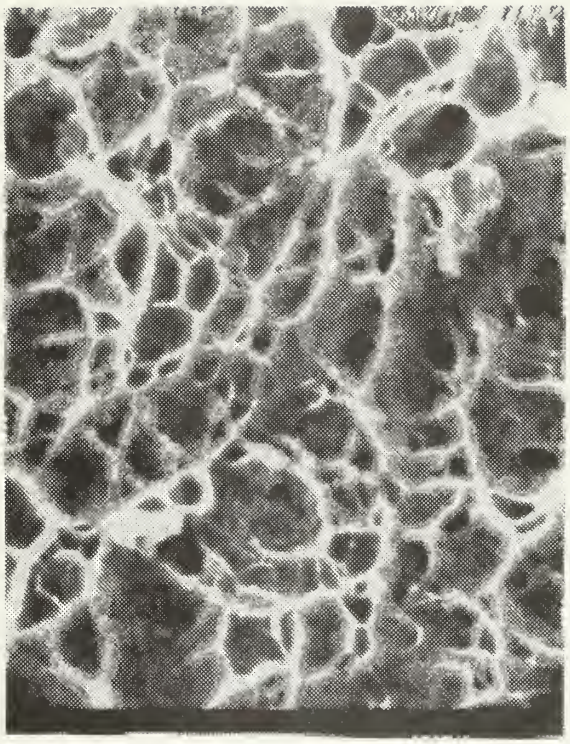

SEM FRACTOGRAPH 9 2400X

Uniformally dimpled structure associated in a bright contrasted fracture surface. Bright contrast in this SEM image on the dimple ridges is indicative of minor tearing.

FIGURE 59. 21-6-9, 195°K, NOTCHED, UNCHARGED

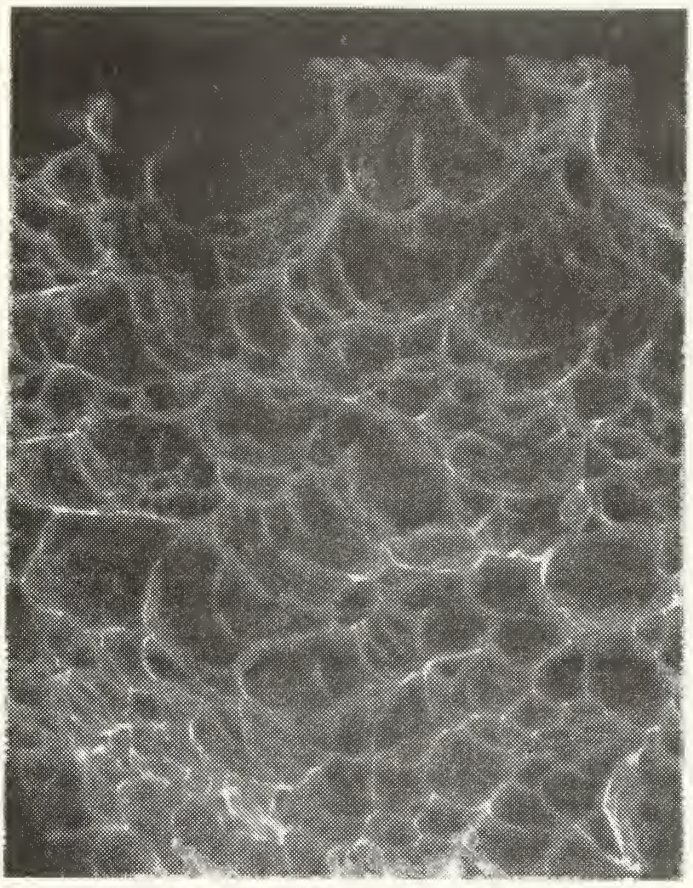

SEM FRACTOGRAPH 36 2300X

Uniformally dimpled structure with some stretching indicated.

FIGURE 60. 21-6-9, 195°K, NOTCHED, 0% ELONGATION PRIOR TO CHARGE

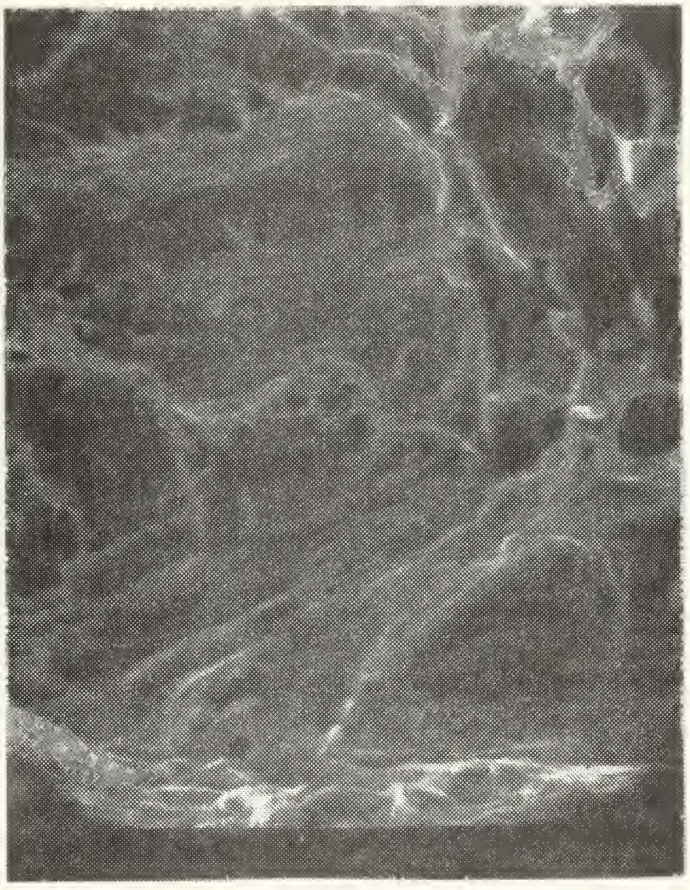

SEM FRACTOGRAPH 37 2300X

Extremely corrugated appearance with minor dimpling. Probably a form of quasi-cleavage. Slight microvoid formation with tearing and stretching indicated.

FIGURE 61. 21-6-9, 195°K, NOTCHED, 4.68% ELONGATION PRIOR TO CHARGE

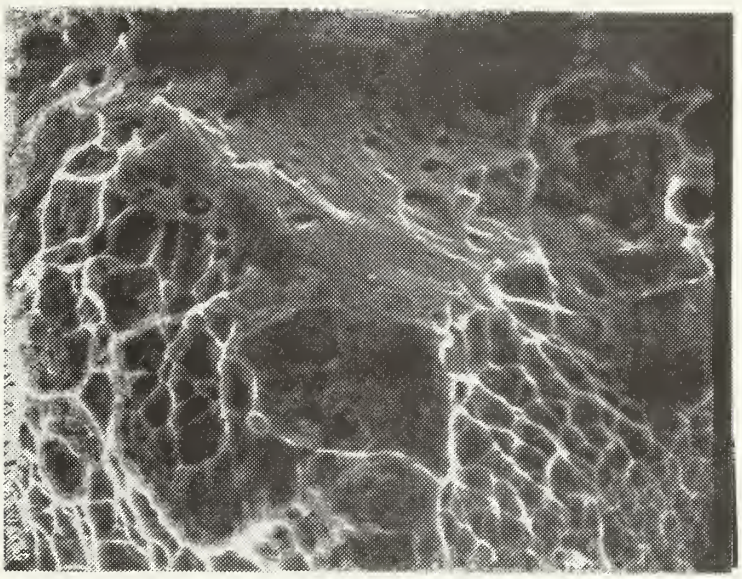

SEM FRACTOGRAPH 11 2400X

Uniformed dimpled structure surrounding a pronounced area of stretching. Tear ridges are interlaced among the dimpled matrix.

FIGURE 62. 21-6-9, 76°K, NOTCHED, UNCHARGED

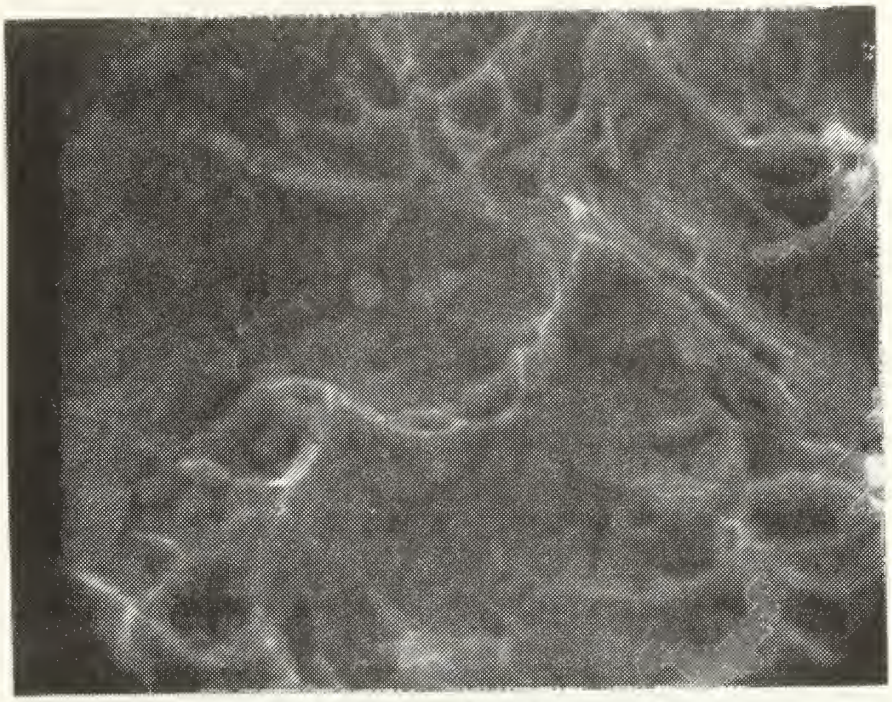

SEM FRACTOGRAPH 41 2500X

Pebbled structure with some minor dimpling. Large spherical inclusion in center. Higher magnification shots indicate definite cleavage facets.

FIGURE 63. 21-6-9, 76°K, NOTCHED, 0% ELONGATION PRIOR TO CHARGE

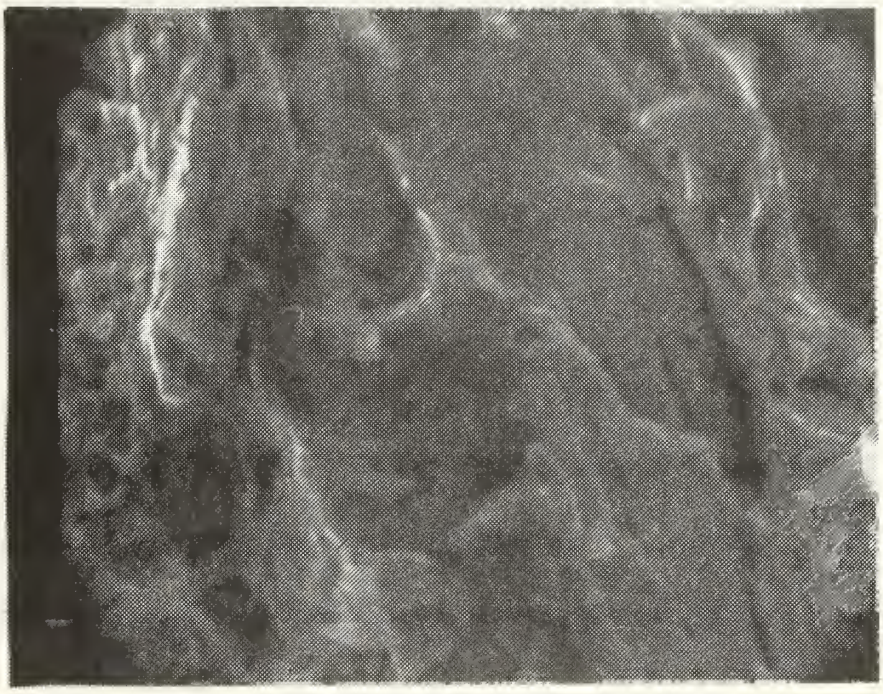

SEM FRACTOGRAPH 41' 2600X

Another view of previous fractured specimen. Definite cleavage features with almost no dimpling. Minor inclusions on fracture surface.

FIGURE 64. 21-6-9, 76°K, NOTCHED, 0% ELONGATION PRIOR TO CHARGE

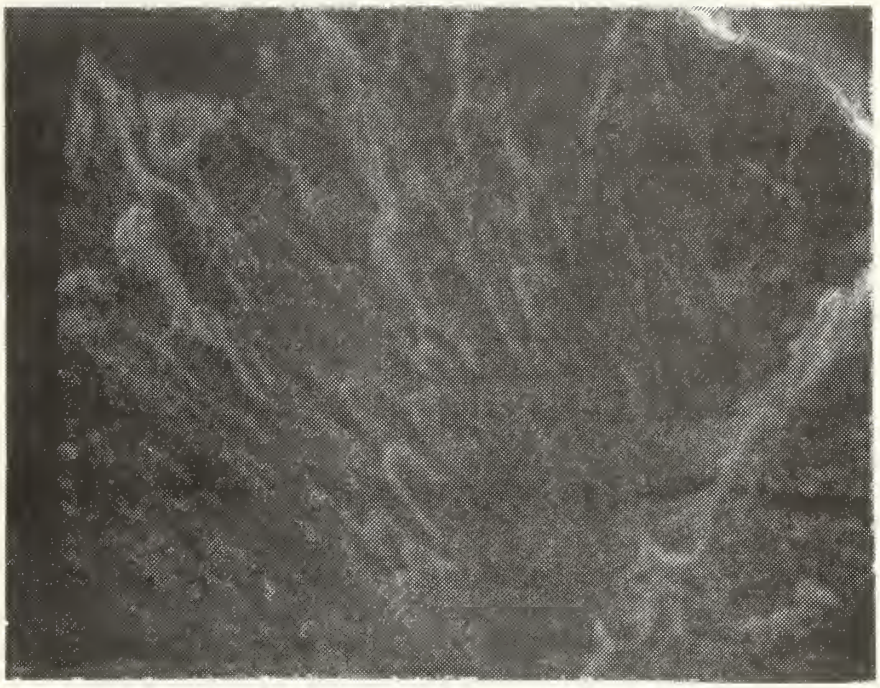

SEM FRACTOGRAPH 42 2300X

Clear evidence of cleavage. Some small dimples near cleavage area.

FIGURE 65. 21-6-9, 76°K, NOTCHED, 2.34% ELONGATION PRIOR TO CHARGE

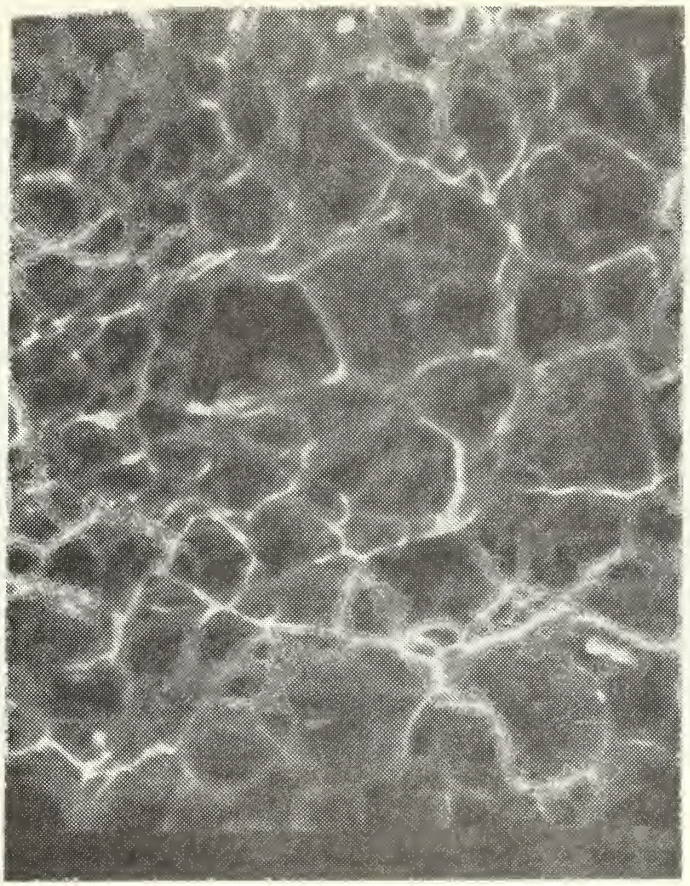

SEM FRACTOGRAPH 42' 2400X

Second view of fracture surface. Numerous dimples have several irregular inclusions at the base. Minor tearing and microvoid formation noted.

FIGURE 66. 21-6-9, 76°K, NOTCHED, 2.34% ELONGATION PRIOR TO CHARGE

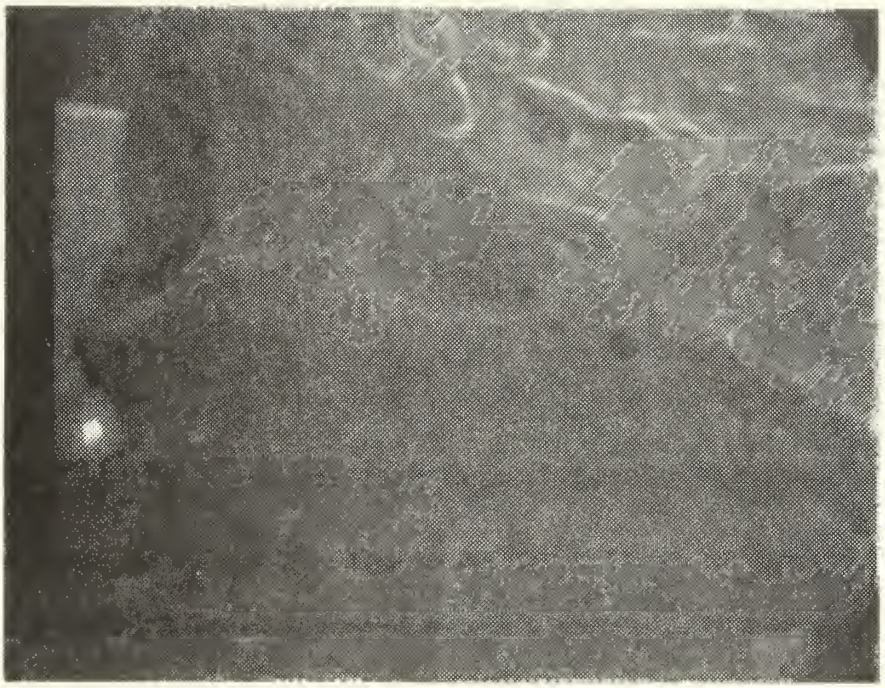

SEM FRACTOGRAPH 42" 2400X

Pebbled structure with some stretched areas and dimples.

FIGURE 67. 21-6-9, 76°K, NOTCHED, 2.34% ELONGATION PRIOR TO CHARGE

TABLE III. FRACTOGRAPHIC SUMMARY TABLE

FIG NO	SEM NO	ALLOY	TEMP.	GEOM	% ELONG PRIOR CHARGE	DIMPLES	LARGE VOIDS	TEAR RIDGES	STRETCH-ING	PEBBLING	CLEAVAGE	NON METALLIC INCLUSIONS
19	2	304-L	300°K	a	0*	◒	—	○	—	○	—	—
20	13	304-L	300°K	a	0	◒	—	○	○	—	—	—
21	14	304-L	300°K	a	17.18	◒	—	○	—	—	—	○
22	15	304-L	300°K	a	35.6	◒	—	◒	○	○	—	○
23	4	304-L	195°K	a	0*	○	—	○	—	○	—	○
24	18	304-L	195°K	a	0	○	—	○	○	○	—	○
25	19	304-L	195°K	a	17.97	○	✓	◒	○	○	○	—
26	20	304-L	195°K	a	31.25	◒	—	○	○	◒	—	○
27	6	304-L	76°K	a	0*	○	—	○	○	○	○	○
28	23	304-L	76°K	a	0	○	✓	○	—	◒	○	○
29	24	304-L	76°K	a	21.88	○	✓	○	○	○	○	○
30	25	304-L	76°K	a	21.81	◒	—	—	◒	—	—	○
31	1	304-L	300°K	b	0*	○	—	○	○	◒	—	○
32	16	304-L	300°K	b	0	—	—	○	○	◒	◒	—
33	17	304-L	300°K	b	7.8	◒	✓	—	◒	—	—	◒

FIG NO	SEM NO	ALLOY	TEMP	GEOM	% ELONG PRIOR CHARGE	DIMPLES	LARGE VOIDS	TEAR RIDGES	STRETCH-ING	PEBBLING	CLEAVAGE	NON METALLIC INCLUSIONS
34	17'	304-L	300°K	b	7.8	◒	✓	—	○	◒	—	●
35	17''	304-L	300°K	b	7.8	◒	✓	—	—	●	—	●
36	3	304-L	195°K	b	0*	◒	—	◒	○	○	—	—
37	21	304-L	195°K	b	0	○	✓	○	●	○	—	—
38	22	304-L	195°K	b	6.25	○	—	○	○	○	—	—
39	5	304-L	76°K	b	0*	◒	✓	○	○	○	—	—
40	26	304-L	76°K	b	0	○	—	—	—	○	◒	○
41	26'	304-L	76°K	b	0	○	—	○	●	○	—	●
42	27	304-L	76°K	b	6.7	○	✓	○	○	○	○	○
43	8	21-6-9	300°K	a	0*	○	—	○	○	●	—	◒
44	28	21-6-9	300°K	a	0	◒	—	○	—	◒	—	—
45	29	21-6-9	300°K	a	14.84	○	—	—	◒	—	—	—
46	30	21-6-9	300°K	a	33.75	◒	✓	○	○	○	—	○
47	10	21-6-9	195°K	a	0*	○	—	○	—	◒	—	○
48	33	21-6-9	195°K	a	0	○	—	○	—	—	○	○
49	34	21-6-9	195°K	a	10.93	○	✓	○	—	—	○	—

FIG NO	SEM NO	ALLOY	TEMP	GEOM	% ELONG PRIOR CHARGE	DIMPLES	LARGE VOIDS	TEAR RIDGES	STRETCH-ING	PEBBLING	CLEAVAGE	NON METALLIC INCLUSIONS
50	35	21-6-9	195°K	a	34.38	○	—	○	○	—	○	—
51	12	21-6-9	75°K	a	0*	○	—	○	—	—	—	—
52	38	21-6-9	75°K	a	0	○	—	○	○	—	○	—
53	39	21-6-9	76°K	a	12.5	○	✓	◒	◒	—	○	○
54	40	21-6-9	76°K	a	32.81	○	✓	○	○	◒	◒	—
55	40'	21-6-9	76°K	a	32.81	○	—	◒	—	—	●	○
56	7	21-6-9	300°K	b	0*	○	✓	○	○	●	—	—
57	31	21-6-9	300°K	b	0	○	—	○	○	●	—	○
58	32	21-6-9	300°K	b	5.93	○	✓	○	○	◒	—	—
59	9	21-6-9	195°K	b	0*	◒	—	◒	○	○	—	○
60	36	21-6-9	195°K	b	0	●	—	○	○	○	—	○
61	37	21-6-9	195°K	b	4.68	○	—	—	○	○	●	○
62	11	21-6-9	76°K	b	0*	◒	—	◒	◒	○	—	○
63	41	21-6-9	76°K	b	0	○	—	○	—	●	◒	◒
64	41'	21-6-9	76°K	b	0	○	—	○	○	◒	●	◒
65	42	21-6-9	76°K	b	2.34	○	—	○	—	◒	●	○

FIG NO	SEM NO	ALLOY	TEMP	GEOM	% ELONG PRIOR CHARGE	DIMPLES	LARGE VOIDS	TEAR RIDGES	STRETCH-ING	PEBBLING	CLEAVAGE	NON METALLIC INCLUSIONS
66	42'	21-6-9	76°K	b	2.34	○	✓	○	—	○	◐	◒
67	42"	21-6-9	76°K	b	2.34	○	—	—	○	◐	—	—

Key

— Denotes None

✓ Denotes Occurrence

○ Denotes Small, Minor, Quasi

◒ Denotes Medium, Average

◐ Denotes Large, Pronounced, Complete

* No Charge

E. METALLOGRAPHIC RESULTS

Selected notched samples of 304-L and 21-6-9 were mounted, polished and etched to determine if any martensitic structure had formed. Because of the variation in composition of these two stainless steels two separate etchants had to be utilized. 21-6-9 required five grams of ferric chloride, 50 ml. of hydrochloric acid and 100 ml. of water. 304-L's etchant consisted of five ml. of nitric acid, one ml. of hydrofluoric acid and 44 ml. of water. Figures 68 and 69 are the result of this study.

F. DISCUSSION OF METALLOGRAPHIC RESULTS

The notched 304-L specimen that was tested at 76°K definitely showed a martensitic structure near the fracture surface. This was determined by the responsiveness of the etchant with a FCC structure and the inability to etch at various random locations in the metal. Because this unetchable structure was distributed throughout the fracture surface, it appears that this transformation had taken place via a strain-induced mechanism rather than being thermally induced by the low temperature.

The metallographic analysis of 21-6-9 indicated that no martensitic structure occurred by deformation and/or by temperature activation. Slip lines are evident throughout the grains of this specimen in a uniform manner.

FIGURE 68. METALLOGRAPHIC PHOTO, 304-L, 76°K, NOTCHED GEOMETRY

FIGURE 69. METALLOGRAPHIC PHOTO, 21-6-9, 76°K, NOTCHED GEOMETRY

VI. CONCLUSIONS

Conclusions drawn from this investigation as to the susceptibility of internal hydrogen embrittlement during low temperature deformation of two austenitic stainless steels are as follows:

1) Prior cold work at temperatures as low as 76°K does not give rise to accentuated susceptibility to hydrogen embrittlement for 304-L and 21-6-9.
2) Cryogenic service which involves molecular hydrogen with low diffusion rates would be much less severe than the cathodic charging procedure employed, so that both materials examined here appear to be favorable for such application. However, the effect of increased austenite instability at liquid hydrogen temperatures must be considered.
3) A strain-induced martensite occurred in the metastable austenitic 304-L alloy at 76°K, and a TRIP EFFECT may have occurred at certain conditions.
4) An apparent ductilizing effect of charging was observed, in some circumstances, but is considered to be due to variations in sample preparation rather than to a true solid solution softening effect.
5) Fractographic evidence indicated that although ductility was present at all temperatures, inclusions became evident only in the charged specimens.

6) "Pebbled" appearances on fracture surfaces occurred mainly in the lower temperature regions and are of an unknown origin.

7) In general both 304-L and 21-6-9 are considered excellent materials for cryogenic applications.

VII. RECOMMENDATIONS

1) Any investigation of the embrittlement of austenitic stainless steels by hydrogen should be limited to only one metal.
2) The time for cathodically charging the specimens should be varied from one to 48 hours. Different current densities should be applied in order to determine optimum embrittling procedure.
3) Sustained load tests such as creep and/or extremely low crosshead rates should be used when testing hydrogen subjected specimens.
4) A method of quickly determining the percent martensite occuring in a sample should be made available during any further investigation regarding ferromagnetic stainless steels. Two methods are described in reference 7 and are easily fabricated.

BIBLIOGRAPHY

1. Gregory, D.P., "The Hydrogen Economy," Scientific American, p. 219-227, January 1973.

2. National Technical Information Service Report Ad 713 619, Crygenic Materials Data Handbook (Revised) Vol. I Sections A, B, C, by F.R. Schwartzberg, et al., p. 463-489, 593-597.

3. Lawrence Radiation Laboratory Report 73293, Tensile and Fracture Properties of Austenitic Stainless Steel 21-6-9 in High Pressure Hydrogen Gas, by R.R. Vandervoort, p. 10-11, 13-16.

4. Bain, E.C., Trans AIME 70, p. 24, 1924.

5. Mangonon, P.F. and Thomas, G., "The Martensite Phases in 304 Stainless Steel," Metallurgical Transactions, p. 1577-1586, June 1970.

6. Batelle Columbus Laboratories Report 646 to University of California Lawrence Livermore Laboratory, Hydrogen in Austenitic Stainless Steels, by E.E. Fletcher, A.R. Elsea, p. 5, 10-12, 24 February 1973.

7. Lawrence Livermore Laboratory Report 51215, The Trip Effect in Fe-Ni-C Alloys, by P.C. Maxwell, J.C. Shyne, and A. Goldberg, p. 22-24, April 1972.

8. Maxwell, P.C., Shyne, J.C., Goldberg, A., "Stress-Assisted and Strain-Induced Martensites in Fe-Ni-C Alloys," Metallurgical Transactions, p. 1305-1318, June 1974.

9. Wickstrom, W.A. and Etheridge, B.R., "Investigation into the Compatibility of Hydrogen and Titanium," Advances in Cryogenic Engineering, Vol. 13, p. 334-342.

10. Defense Metals Information Center Report 196, Hydrogen-Induced, Delayed, Brittle Failures of High-Strength Steels, by A.R. Elsea and E. E. Fletcher, p. 57, 106-114, January 1964.

11. Metallurgical Society Conferences, Fracture of Solids, Vol 20, "The Hydrogen Embrittlement of Ferrous Alloys," by A.S. Tetelman, p. 671-707, August 1962.

12. Latanision, R.M. and Opperhauser, H., "The Intergranular Embrittlement of Nickel by Hydrogen: The Effect of Grain Boundary Segregation," Metallurgical Transactions, p. 483-491, February 1974.

13. Chandler, W.T. and Walter, R.J., "Hydrogen Environment Embrittlement of Metals and Its Controls," Miami Energy Conference, p. 56-15 - 56-31, 16-20 March 1974.

14. Defense Metals Information Center Report 219, Hydrogen Movement in Steel-Entry, Diffusion, and Elimination, by E.E. Fletcher and A.R. Elsea, p. 16-38, June 1965.

15. Louthan, M.R., Donovan, J.A. and Caskey, G.R., Tritium Absorption in 304-L Stainless Steel, paper presented at AIME-IMD Meeting, Detroit, Michigan, October 1974.

16. Martin Marietta Laboratories Report 74-07c, Electrochemical Techniques in the Study of Embrittlement Phenomena, by J.A.S. Green and R.M. Latanision, p. 1-12, February 1974.

17. Phone conversation dated 15 August 1974.

18. Louthan, M.R. and Derrick, D.G., "Hydrogen Transport in Austenitic Stainless Steels," to be published in Corrosion Science.

19. Carter, S.F., "Effect of Melting Practice on Hydrogen," Proc. Elec Furn Steel Conference, 1949.

20. Ravi, K.V. and Gibala, R., "The Strength of Niobium-Oxygen Solid Solutions," Acta Metallurgica, p. 623-633, June 1970.

21. Tanaka, T., "On the Solid Solution Softening in Fe-2.8 at % Ni and Fe-2.9 at % Si," Scripta Metallurgica, p. 97-103, January 1973.

22. Ravi, K.V. and Gibala, R., "The Strength and Alloy Softening of BCC Metals," Scripta Metallurgica, p. 547-551, August 1969.

INITIAL DISTRIBUTION LIST

		No. Copies
1.	Defense Documentation Center Cameron Station Alexandria, Virginia 22314	2
2.	Library, Code 0212 Naval Postgraduate School Monterey, California 93940	2
3.	Department Chairman, Code 59 Department of Mechanical Engineering Naval Postgraduate School Monterey, California 93940	1
4.	Professor A.J. Perkins, Code 59Ps Department of Mechanical Engineering Naval Postgraduate School Monterey, California 93940	5
5.	Professor G.R. Edwards, Code 59Ed Department of Mechanical Engineering Naval Postgraduate School Monterey, California 93940	5
6.	LCDR P.F. Scardigno, USN 117 White Chapel Drive Benicia, California 94510	5

Thesis
S243 Scardigno
c.1 The relation of low temperature deformation and susceptibility to hydrogen embrittlement of austenitic stainless steels.

157040